Advancing geodynamic research in Antarctica: Reprocessing GNSS data to infer consistent coordinate time series (GIANT-REGAIN)

Eric Buchta[1], Mirko Scheinert[1], Matt A. King[2,5], Terry Wilson[3], Achraf Koulali[4], Peter J. Clarke[4], Demián Gómez[3], Eric Kendrick[3], Christoph Knöfel[1,6], and Peter Busch[1,7]

[1]Institut für Planetare Geodäsie, TUD Dresden University of Technology, Dresden, Germany
[2]School of Geography, Planning, and Spatial Sciences, University of Tasmania, Tasmania, Australia
[3]School of Earth Sciences, The Ohio State University, Columbus, USA
[4]Geospatial Engineering, School of Engineering, Newcastle University, Newcastle, UK
[5]The Australian Centre for Excellence in Antarctic Science, University of Tasmania, Tasmania, Australia
[6]now at: Federal Agency for Cartography and Geodesy, Frankfurt/Main, Germany
[7]now at: Vodafone Group Services GmbH, Düsseldorf, Germany

Correspondence: Eric Buchta (eric.buchta@tu-dresden.de)

Abstract. For nearly three decades, geodetic GNSS measurements in Antarctica have provided direct observations of bedrock displacement, which is linked to various geodynamic processes, including plate motion, post-seismic deformation and glacial isostatic adjustment (GIA). Previous geodynamic studies in Antarctica, especially those pertaining to GIA, have been constrained by the limited availability of GNSS data. This is due to the fact that GNSS data are collected by a wide range of institutions and network operators, with the raw observational data either not publicly available or scattered across various repositories. Further, the metadata necessary for rigorous data processing has often not been available or reliable. Consequently, the potential of GNSS observations for geodynamic studies in Antarctica has not been fully exploited yet. Here, we present consistently processed coordinate time series for GNSS sites in Antarctica and the sub-Antarctic region for the time span from 1995 to 2021. The data set is composed of 286 continuous and episodic sites, with 258 sites having a time span longer than three years. The coordinate time series were obtained from a combination of four independent processing solutions using different GNSS software and products, allowing the identification of inconsistencies in individual solutions. From these, we infer a reliable and robust combined solution. A key issue was the thorough reassessment of station metadata to minimise artefacts and biases in the coordinate time series. The resulting data set provides coordinate time series with unprecedented spatio-temporal coverage, promising significant advancements in future geodynamic studies in Antarctica.

1 Introduction

The deformation of the solid Earth is caused by a multitude of geodynamic processes that occur on different temporal and spatial scales. Measurements using geodetic GNSS on bedrock were first conducted in Antarctica in the mid-1990. These have proven to be highly effective for determining bedrock displacement to quantify and characterise underlying geodynamic processes, such as the determination of plate motion (Bouin and Vigny, 2000; Dietrich et al., 2001, 2004; Savchyn et al., 2023), the assessment of post-seismic deformation (King and Santamaría-Gómez, 2016; Nield et al., 2023), the validation of

ocean tide models (King et al., 2005) or studies of local deformation due to volcanism (Grapenthin et al., 2022). In terms of current research, deformation processes originating from the interaction of the solid Earth with the Antarctic Ice Sheet (AIS), which manifest themselves predominantly as vertical bedrock displacement, are of greatest importance. Here, traditionally a distinction is made between the instantaneous, elastic response of the solid Earth to contemporary ice mass changes caused by dynamic ice mass loss and variations in the surface mass balance (SMB) (Koulali et al., 2022), and the visco-elastic response to past ice-ocean loading changes - known as glacial isostatic adjustment (GIA).

The determination of GIA plays a prominent role in current climate research (King et al., 2010). Gravity observations from the GRACE and GRACE-FO missions are used to determine the mass change of the AIS (King et al., 2012; Groh and Horwath, 2021; Otosaka et al., 2023) and consequently its contribution to current sea-level rise. Here, the standard procedure involves a reduction of the GRACE observations by the mass effect of GIA, to isolate the mass signals of present-day ice-mass change. However, both inverse and empirical GIA models differ significantly in their spatial pattern and amplitude (Martín-Español et al., 2016; Whitehouse, 2018), making the GIA correction the largest contributor to the uncertainty of estimated ice mass changes from GRACE and GRACE-FO observations (Otosaka et al., 2023).

A multitude of studies employed GNSS observations to ascertain GIA-induced vertical rates on regional (Bevis et al., 2009; Argus et al., 2011; Scheinert et al., 2006; Zanutta et al., 2017; Hattori et al., 2021; King et al., 2022) and continental scale (Thomas et al., 2011; Argus et al., 2014; Rülke et al., 2015; Liu et al., 2018; Li et al., 2022). Regional studies can make an important contribution to highlight local or regional deficiencies of GIA models. For example, King et al. (2022) utilised GNSS observations to report on widespread rates of subsidence in the East Antarctic region between 77°E and 120°E, after correcting for SMB induced variations and common mode errors, which are not included in any GIA forward model. King et al. (2022) suggested shortcomings in the assumed ice-load history, postulating a late Holocene re-advance of the ice sheet in the region west of Denman Glacier. In West Antarctica, the Amundsen Sea region exhibits particularly high uplift rates of up to $60 \, \mathrm{mm \, yr}^{-1}$ with steep spatial gradients (Groh et al., 2012; Busch et al., 2017; Barletta et al., 2018), which are not reflected in most GIA models. Barletta et al. (2018) used GNSS observations to derive a regional GIA model, obtaining a low-viscosity of the upper mantle ranging from just $4 \times 10^{18} \, \mathrm{Pa \, s}$ to $2.5 \times 10^{19} \, \mathrm{Pa \, s}$. The derived upper mantle viscosity is two to three orders of magnitude lower than that typically used for GIA models covering whole Antarctica, resulting in a significantly reduced GIA response time to ice mass changes of just decades to centuries. A similarly low viscosity mantle was identified using GNSS and models in the northern Antarctic Peninsula (Nield et al., 2014; Samrat et al., 2020, 2021).

Given the diversity of spatio-temporal patterns inherent in various geodynamical processes, the requirements for a comprehensive data set inferred from GNSS time series to observe these processes are manifold:

– To accurately assess the GIA effect on a continental scale as well as signals with smaller spatial wavelengths it is essential to provide a data set with the best possible spatial coverage both in extent and resolution.

– To correctly resolve non-linear geodynamic processes (Nield et al., 2014; Liu et al., 2018; Koulali et al., 2022; Nield et al., 2023) it is necessary to produce time series with a sufficient temporal resolution, typically daily resolution. To derive accurate secular rates, or detect changes in rates, one aims to maximise the time span of the GNSS time series.

55   – To allow for an assessment of GIA models on the accuracy level of $1\,\mathrm{mm\,yr^{-1}}$, highly consistent and accurate data are required. As demonstrated by Martín-Español et al. (2016), a GIA model error of $1\,\mathrm{mm\,yr^{-1}}$ integrated over the area of East Antarctica translates into a mass effect of $45\,\mathrm{Gt\,yr^{-1}}$ which is equivalent to the magnitude of the signal itself.

Presently, no data set can be considered to fulfil the above points to the best possible extent. The reasons are manifold. While for some large GNSS networks the observation data are freely accessible, e.g. the POLENET network (The Polar Earth Observing

60 Network) (Wilson et al., 2019) or the IGS network (International GNSS Service) (Johnston et al., 2017; Vardić et al., 2022), the observation data of smaller networks or individual stations are either scattered over various repositories or are not freely accessible. In particular, historic campaign/episodic measurements are often unavailable even though they can greatly enhance the spatial coverage of a data set. Metadata, i.e. information on the site setup, are essential to determine consistent coordinate time series but are often insufficiently documented, especially for past (mostly episodic) sites and measurement campaigns,

65 leading to potential misinterpretation of derived coordinate trajectories. Coordinate time series data sets produced with a high degree of automation such as those provided by the Nevada Geodetic Laboratory (NGL) (Blewitt et al., 2018) rely on metadata stored in the observational RINEX files (Receiver Independent Exchange Format), which can be prone to errors. The combination of coordinate time series or displacement rates derived from heterogeneous or independent studies (e.g. combining regional and continent-wide studies) is not advisable, since different studies rely on differing processing conventions, like

70 the adopted reference frame or specific geophysical reductions, resulting in an inconsistent data set. Before realising a data combination of this kind, a consistent processing of all observation data is mandatory.

To exploit the full potential of GNSS observations in Antarctica, the SCAR (Scientific Committee on Antarctic Research) -endorsed project GIANT-REGAIN (Geodynamics In ANTarctica based on REprocessing GNSS dAta Initiative) was initiated which aimed for the acquisition and consistent processing of all available GNSS recordings on bedrock in Antarctica for the

75 period from 1995 to 2021. Here we present the results of the GIANT-REGAIN project providing coordinate time series as the main product. We report on the acquisition of observational data that originate from more than twenty different networks and institutions, including freely accessible data and data from past measurement campaigns. We could especially obtain observational data from previously unpublished GNSS sites. The relevant site metadata, which are indispensable for the correct assignment of the hardware setup, were re-evaluated and, if necessary, corrected.

80 The observational data were processed by four contributing analysis centers (ACs), namely Dresden University of Technology (TUD), University of Tasmania (UTAS), Ohio State University (OSU) and Newcastle University (NEWC). The inclusion of multiple independent ACs allows us to evaluate the processing noise, especially:

    – to validate and detect inconsistencies in the individual solutions;

    – to assess systematic differences (biases) in the resulting coordinate time series on different temporal scales;

85   – to assess and compare noise characteristics of the individual coordinate time series.

Subsequently, the individual coordinate time series were used to form a combined final data set. This is beneficial as not all centers produced solutions for every site-day. Thus, the combination enables us to maximise the spatio-temporal coverage

compared to the individual solutions while preserving the noise level of the individual solutions. The final data set comprises coordinate time series for 286 GPS sites. This data set provides, therefore, the most comprehensive spatio-temporal coverage ever for Antarctica. Equipment changes can alter the trajectory of GPS coordinate time series. We rigorously revised the meta-data records for all sites within our data set to ensure the correct interpretation of the coordinate time series w.r.t. to geodynamic processes. Clear and accurate metadata records also allow for a best possible inter-centre consistency and provide a reliable foundation for future reprocessing. Furthermore, GPS sites with a missing or incomprehensible metadata record as well as sites showing clear monument instability in their coordinate trajectory were not considered for the final product.

We compared our resulting coordinate time series to the latest data set provided by the Nevada Geodetic Laboratory (NGL) (Blewitt et al., 2018) which provided, until present, the most extensive record of processed GNSS coordinate time series in Antarctica. This is a convenient and widely used open-access data set, widely used in several recent studies (Li et al., 2022; Savchyn et al., 2023). We assess differences between the data sets on secular time scales (linear rates), and demonstrate the impact of the updated GIANT-REGAIN metadata information on adopted antenna heights.

2 Data acquisition

2.1 Observational data

The primary objective of this study is to analyse and provide a data set that includes all GNSS observations on bedrock for the period 01/1995 to 12/2021. Before going into detail, we want to briefly emphasize the usage of the terms GNSS and GPS. The first GNSS deployments tracked only GPS satellites. Many of these sites have since been upgraded with receivers capable of tracking multi-GNSS constellations, making it more correct to refer to these specific sites as GNSS stations. However, the processing strategies applied in this study were limited to GPS observations, resulting in coordinate time series based on GPS-only observations. Therefore, we use the terms GPS stations and GPS coordinate time series throughout the rest of this paper. The required GPS observational data, in the form of raw binary files or the RINEX format, were as far as possible obtained from publicly accessible repositories. The Geodetic Facility for the Advancement of Geoscience (GAGE) manages the observational data and metadata for POLENET-associated stations and make them publicly available. Observational data for GPS sites contributing to the global IGS network are made publicly available via multiple repositories (e.g. the CDDIS - Crustal Dynamics Data Information System). The observational data from smaller networks or past measurement campaigns are included in GAGE or scattered over smaller data repositories or are not publicly available at all (see supplement Tab. S1 for the complete list of DOI listed observational data).

Following a first call for data contribution by the initiators of the GIANT-REGAIN project in 2016, more than twenty station operators and national Antarctic research programs supported the provision of GPS data for this project. This included stations with already processed and published time series as well as GPS stations with so far unpublished coordinate time series. Fig. 1 provides an overview of the spatial distribution of the GPS sites and their associated networks. To observe geodynamic processes related to solid Earth deformation, the measurements need to refer to specifically marked points in the bedrock. With

only 0.18 % of the Antarctic continent consisting of ice-free bedrock (Burton-Johnson et al., 2016), suitable locations for GPS sites are limited to the coastal regions and mountain ranges.

Antarctic GPS sites have been occupied in two ways: campaign-style with episodic measurements (eGPS) and as continuously operating installations (cGPS). Episodic measurements are realised using the antenna on a fixed marker in the bedrock, with equipment removed at the end of each campaign and reinstalled after an interval typically of a year or more. Occupations typically last a few days to a few weeks.

The first cGPS sites were set up near research stations in the early and mid-1990s. These sites contribute to the global IGS network (Johnston et al., 2017) and provide the longest and most complete observation record within this study. The IGS sites were set up at staffed Antarctic stations, namely Casey (CAS1), Mawson (MAW1), Dumont d'Urville (DUM1), Davis (DAV1), McMurdo (MCM4) and Syowa (SYOG). Later additional sites were incorporated into the IGS network, such as Scott Base (SCTB), Mt. Coates (COTE), O'Higgins (OHI2, OHI3), Arrival Heights, McMurdo (ARHT), Rothera (ROTH), Palmer Station (PALM), while other sites lost their IGS status (Vesleskarvet, VESL) or were decommissioned (PALV, OHIG).

Starting in 1995, several projects were launched to establish additional regional and local GPS networks. The SCAR Epoch Crustal Movement Campaigns from 1995 to 1999 focused on the regions of the Antarctic Peninsula and Dronning Maud Land, and comprised coordinated episodic measurements with contributions and support from several national polar programs (Dietrich et al., 2001, 2004). The TAMDEF (Transantarctic Mountains Deformation) project, with its first observations in 1996, established a GPS network covering large parts of the Transantarctic Mountains, consisting of 25 episodic, six quasi-continuous and two continuous sites (Raymond et al., 2004; Vázquez Becerra, 2009). The first sites of the VLNDEF (Victoria Land Network for DEFormation Control) network were installed during field campaigns in 1999/2000 and 2000/2001 (Zanutta et al., 2017, 2018) with 28 sites in the final configuration. The WAGN (West Antarctic GPS Network) was operated between 2001 and 2006 and covered yet unobserved regions of West Antarctica (Bevis et al., 2009). A small GPS array of episodic sites was installed in the region of western Marie Byrd Land over 1999-2002 (Donnellan and Luyendyk, 2004) and around the Amery Ice Shelf in East Antarctica Tregoning et al. (1999, 2000).

The harsh Antarctic conditions, such as low temperatures and the polar night, introduce particular technological and logistical challenges to the establishment and maintenance of GPS stations. Establishing a continuous and resilient energy supply has posed significant problems. Undertaking maintenance work presents a significant logistical challenge, and data transfer must be accomplished either remotely or through manual collection. An essential increase in the spatial coverage of remote cGPS was achieved following the International Polar Year (IPY) from 2007 to 2009 (see Fig. 1b). The POLENET embedded network ANET formed the nucleus of the initiative. The ANET network extends from Victoria Land to the Amundsen Sea Embayment and Filchner-Ronne Ice Shelf, covering major parts of West Antarctica. Within the POLENET initiative some of the previous eGPS sites of the WAGN, TAMDEF and Marie Byrd Land network were reoccupied and upgraded to cGPS sites. International partners contributed to the ANET network. Three sites of the VLNDEF (VL01, VL12 and VL30) network were upgraded to cGPS sites and included in the POLENET network in the season 2014/2015 (Zanutta et al., 2017). The POLENET-UKANET network of cGPS sites covers large parts of the Antarctic Peninsula and the surroundings of the Filchner-Ronne Ice Shelf (Whitehouse et al., 2020). It includes sites of the LARISSA (LARsen Ice Shelf System, Antarctica) network, consisting of

six cGPS sites (installed in 2008 and 2010) covering the northern part of the Antarctic Peninsula (Nield et al., 2014) and the CAPGIA (Constraints on Antarctic Peninsula GIA) network (King et al., 2013; Wolstencroft et al., 2015) installed in the Antarctic summer season 2009/2010 which consists of nine cGPS sites. In addition to these large-scale networks, there exist networks with smaller spatial extent operated by various institutions. TU Dresden continues to operate eGPS stations in the area of the Antarctic Peninsula, in Dronning Maud Land and the Amundsen Sea Embayment, which in part represent the continuation of the initial measurements of the SCAR Epoch Crustal Movement Campaigns (Rülke et al., 2015; Scheinert et al., 2023). The Japanese Antarctic Research Expedition (JARE) operates a local network at the Lützow-Holm Bay (37°E – 40°E and 69°S – 70°S) (Hattori et al., 2021). In addition to the IGS station SYOG, episodic measurements were initially carried out and later partially upgraded to cGPS stations (the observational data from the cGPS stations were not available for this study). King et al. (2022) installed a network of six cGPS sites, providing observations for the so far barely covered coastal area of East Antarctica between Davis and Casey Stations (70°E – 120°E). Observational data from five sites were available for this study. Several sites are not affiliated to larger networks and are often co-located to research stations (e.g., ABOA (Andrei et al., 2018), NONS, SVEA, KOH2, VESL, LXAA). These sites can contribute significantly to an increased spatial coverage, especially in East Antarctica where the coverage is otherwise very sparse. The number of daily observations within Antarctica had increased steadily since 1995 (Fig. 1b) with a significant increase in 2008 with the initiation of the POLENET project. The peak number of daily site observations (100) was reached in 2016 and has remained somewhat steady afterwards. However, the observation count decreased in 2020, partly due to the COVID pandemic, when maintenance work and manual data retrieval were not possible for some sites.

2.2 Metadata

Correct metadata are essential to determine consistent time series from GPS. In the context of GPS data processing, the metadata contains information about the hardware setup. Incorrect information can lead to biased, more noisy time series and subsequently to errors in derived deterministic parameters, such as linear trends. Correct metadata are of utmost importance for eGPS (Scheinert et al., 2023), since errors in the metadata (e.g. antenna heights) can bias measurement campaigns and are not necessarily detectable by the analysis of the coordinate trajectories (depending on the number of measurements).

Basic information are usually provided in the RINEX header section and include, among others, information about the installed antenna (type, serial number), receiver (type, serial number, firmware version) and antenna eccentricities. For past sites, the RINEX header often contains incomplete or even false information. For this study, we confirmed or corrected the metadata information, using metadata logs, observation protocols, images of the GPS stations (with a focus on the antenna setup), published metadata information, or personal communication with site operators.

To ensure the reproducibility of the processing and to enable possible future reprocessings, the metadata are provided in the established and comprehensive format of the station log files [1] of the IGS (Buchta et al., 2024d).

Multiple studies (Argus et al., 2014; Konfal et al., 2016; Koulali and Clarke, 2020) reported on the effect of snow intrusion into the GPS antenna radomes through drainage holes in the ground plates for a subset of ANET and UKANET cGPS sites,

---

[1]https://files.igs.org/pub/station/general/sitelog_instr.txt, last visited 15 July 2024

leading to offsets and quasi-periodic (annual) signals in the coordinate time series. As a countermeasure, the drainage holes were initially closed with tape and later sealed with permanent plugs. A comprehensive list of efforts regrading the sealing of drainage holes was provided for this study (pers. comm., D. Saddler, OSU, 11 October 2023). Understanding the sealing efforts is crucial for accurately interpreting the coordinate time series, as this can significantly alter the coordinate trajectory. The efforts on antenna sealing are listed within the auxiliary data published in conjunction with the coordinate time series (Buchta et al., 2024c).

3 GPS processing

The data processing involved three major steps. First, the four analysis centres processed the provided observation data, considering the associated, consistent set of station metadata. Second, the resulting time series were transformed using a rigid body (six parameter Helmert) transformation to align the coordinates to a common set of selected regional IGS core sites (see Sect. 3.2.1). This minimises biases in the secular time scales of the individual solutions. Third, the final set of coordinate time series was computed by combining the transformed time series station by station.

3.1 GPS processing of individual AC solutions

The individual analysis methods of the ACs differ in the analysis software, the processing strategies (e.g. double differencing or zero differencing), auxiliary products, and the strategies to realise the terrestrial reference frame, while all ACs adopted the same version of the ITRF to ensure consistency. At the time of the initial processing, the latest version, the ITRF2020 (Altamimi et al., 2023) was not available. Therefore, all ACs realised the IGb14 reference frame, the GNSS-only realisation of the ITRF2014 (Altamimi et al., 2016), and adopted the associated absolute antenna corrections for satellite and ground antennas provided by the IGS (igs14.atx). As mentioned in sec. 2.1, we did not include observations of all GNSS, but restricted our analysis to GPS observations.

The TU Dresden (TUD) analysis centre adopted a standard network processing approach based on double-differenced phase observations using the Bernese GNSS Software v5.2 (Dach et al., 2015). The Antarctic GPS network was processed together with a selection of long running IGS sites surrounding Antarctica. Satellite orbits and Earth rotation parameters were fixed to final products provided by the Center for Orbit Determination in Europe (CODE) (Sušnik et al., 2016). A-priori zenith path delays (ZTD) were realised by employing the dry ZHD (hydrostatic delay in zenith) and the Vienna Mapping Function (VMF3) (Landskron and Böhm, 2018). In order to apply the VMF3 a modified version of Bernese GNSS Software v5.2 was used. The ZTD was parameterised as a piece-wise linear function with one hour resolution. A horizontal tropospheric gradient was estimated once a day. First order ionospheric effects were mitigated by forming the ionospheric-free linear combination. Second-order and third-order ionospheric effects were considered, based on global ionosphere maps (GIM) provided by CODE. Ocean tidal loading corrections and atmospheric tidal loading corrections were applied on the observation level using the ocean tide model FES2014b (Lyard et al., 2021) and the atmospheric tide model of Ray and Ponte (2003), respectively. Non-tidal loading corrections were not applied. Solid Earth tide and solid Earth pole tide corrections were applied according to

the IERS2010 conventions (Luzum and Petit, 2012). Only observations above 5° elevation were considered. Phase ambiguities were fixed to integers if possible, using a sophisticated scheme of baseline-length dependent strategies (Dach et al., 2015). The Bernese Software v5.2 allows to consider the misalignment of ground antennas from true north. If the station meta data include information on the antenna orientation, the azimuth-dependent phase center corrections were applied accordingly. This does not apply to reference stations to maintain consistency with the IGb14 conventions. The geodetic datum was defined using a minimum-constraint approach imposing a no-net translation (NNT) condition on a set of regional IGS core stations w.r.t. the IGb14 reference frame, when solving the daily normal equations for station coordinates and tropospheric parameters.

The University of Tasmania (UTAS) AC analysed the GPS data using the GIPSY v6.4 software (Webb and Zumberge, 1995) and non-fiducial NASA Jet Propulsion Laboratory (JPL) orbit and clock products (repro3). A zero-differenced precise point positioning (PPP) methodology was adopted (Zumberge et al., 1997). Pseudorange data were phase-smoothed and all data were downsampled to $300\,\mathrm{s}$ interval. Only observations above 10° elevation were used. Receiver clock corrections were estimated every $300\,\mathrm{s}$ as a white noise process. Wet tropospheric zenith delays and gradients were estimated every $300\,\mathrm{s}$ with a random walk process noise of $5 \times 10^{-8}\,\mathrm{km\,s^{-0.5}}$ and $5 \times 10^{-9}\,\mathrm{km\,s^{-0.5}}$, respectively (Bar-Sever et al., 1998). The gridded VMF1 tropospheric mapping function was used, with hydrostatic and a priori zenith wet delays extracted from these grids which were based on ECMWF (European Centre for Medium-Range Weather Forecasts) products (Boehm et al., 2006; Kouba, 2008). Second-order ionospheric effects were corrected based on JPL IONEX files from year 1999 onwards. Solutions prior to 1999 instead used the International Reference Ionosphere model. A shell height of $600\,\mathrm{km}$ was used in both cases (Kedar et al., 2003). Solid Earth tide and solid Earth pole tide corrections were made as per the IERS2010 conventions (Luzum and Petit, 2012). Ocean tidal loading displacements were modelled based on the TPXO7.2.2010 ocean tide model in the CM frame as is appropriate for JPL orbits which are also in a CM frame (Fu et al., 2012), with 342 companion tidal constituents computed using the hardisp program (Luzum and Petit, 2012). Ambiguities were fixed to integers where possible (Bertiger et al., 2010). Daily site coordinates were then transformed from the fiducial-free frame of the orbits to the IGS14 using the JPL 7-parameter transformation files.

The Ohio State University (OSU) processing was performed with double differences in "GPS At MIT/Global Kalman filter" (GAMIT/GLOBK) software 10.71 (Herring et al., 2016) using the Ohio State High Performance Computer facility and a paralellised Python wrapper for GAMIT known as Parallel.GAMIT[2]. The GPS data were processed using the IGS14 final orbits.VMF1 grids (Boehm et al., 2006) were used with piece-wise linear functions of one hour resolution to estimate the atmospheric delay. FES2014b (Lyard et al., 2021) was applied to correct for ocean tidal loading. The Antarctic data was processed together with a regional network spanning most of the southern hemisphere to improve ambiguity resolution and network stability. Due to the large number of stations, we split the processing into sub-networks of about 40 sites which include stations from a daily "backbone" network (of about 50 sites with an aperture that spans the entire region of interest) and up to 9 stations from neighboring sub-networks. The daily solutions of the sub-networks were combined using GLOBK to produce daily GPS polyhedrons. The IGb14 frame was realised following the regional methodology of Gómez et al. (2022), where position, velocity, and seasonal (periodic) parameters were inherited from the parent frame (60 stations of the IGb14) using a highly

---

[2]available through GitHub: https://github.com/demiangomez/Parallel.GAMIT

255 consistent combination of daily solutions of about 400 stations.

The NEWC Antarctic Center analysed GPS observables using the "GPS At MIT/Global Kalman filter" (GAMIT/GLOBK) software 10.70 (Herring et al., 2016). The GAMIT software employs double-difference network solutions based on ionospheric-free linear combination of GPS observables to mitigate phase biases resulting from errors in receiver and satellite clocks. The NEWC Antarctic processing strategy is similar to Koulali and Clarke (2020), utilising a two-step approach (Dong et al., 1998).

260 In the first step, GPS phase observations from each day were used to generate loosely constrained position and covariance solutions. The solutions obtained from the first step were then utilised in the second step within the Kalman filter to estimate a consistent set of coordinates, time series, and velocities. Satellite orbit parameters remained fixed to the IGS final repro3 orbit product values. This might introduce a small scaling effect due to the inconsistency of the repro3 product series with IGb14 and igs14.atx. Second-order ionospheric corrections were applied using the combined IGS IONEX files. The zenith wet delay

265 (ZWD) was modelled using a piece-wise linear function with process noise uncertainty constraint of $20\,\mathrm{mm\,h^{-0.5}}$, with three N/S and E/W atmospheric gradients per day. We implemented the time-varying a priori Zenith Hydrostatic Delay (ZHD) and Vienna Mapping Function (VMF1), derived from the ECMWF model (Boehm et al., 2006). An elevation cut-off angle of $10°$ was used, and observations were weighted using an elevation-dependent scheme based on the post-fit residuals. We considered the effects of ocean tide loading by using the FES2014 model (Lyard et al., 2021). Non-tidal atmospheric pressure loading

270 (NTAL) deformation was considered on the observational level (Tregoning and Watson, 2009). We determined the deformation from VMF1 grids of the atmospheric pressure by convolution in the spatial domain using Green's functions in the CM frame. In order to ensure consistency with the solutions of the other ACs, the mean daily NTAL deformation was restored to the final coordinate time series. To perform a double-difference solution in GAMIT, a network of stations needs to be defined. For computational efficiency, the NEWC Antarctic network was divided into seven sub-networks, each containing up to 45

275 stations. The stations in each sub-network were chosen based on geographic location to minimise station baseline lengths, which improves integer phase ambiguity resolution. IGS tie stations, which are common to all sub-networks, were included to allow the combination of the sub-networks into a single full-network solution using GLOBK. To ensure past data integrity, a set of 40 global IGS stations is included for processing data before the year 2000, enhancing ambiguity resolution. In addition to Antarctic networks, we processed a global network based on IGS14 core stations, facilitating the integration of all subnetworks

280 into a unified network solution using the GLOBK Kalman filter. Daily solutions were aligned with the ITRF2014 reference frame through estimation of rotations and translations, minimising position residuals at specified reference frame stations.

3.2 Strategy to infer combined coordinate time series

3.2.1 Transformation to a common frame

To ensure maximum consistency when combining the individual coordinate time series, biases between the solutions were

285 assessed and, if necessary, minimised. Each daily set of station coordinates from an AC j solution $\boldsymbol{X}_j(t)$ is related to a regional set of IGb14 core sites (Fig. 2) via a 6-parameter Helmert transformation:

$$\boldsymbol{X}_{I14}(t) = \boldsymbol{R}_z(\gamma(t)) \cdot \boldsymbol{R}_y(\beta(t)) \cdot \boldsymbol{R}_x(\alpha(t)) \cdot (\boldsymbol{X}_j(t) + \boldsymbol{T}(d_x(t), d_y(t), d_z(t))). \tag{1}$$

We estimated three translation parameters $d_x(t)$, $d_y(t)$, $d_z(t)$ and three rotation parameters $\alpha(t)$, $\beta(t)$, $\gamma(t)$ for each day t and each AC solution j by minimising the square sum of the differences between the daily coordinate solution $\boldsymbol{X}_j(t)$ and the reference coordinates $\boldsymbol{X}_{I14}(t)$ given by the IGb14. If the post-fit residuals of a potential reference site exceeded the limits of $15\,\mathrm{mm}$, $15\,\mathrm{mm}$ or $30\,\mathrm{mm}$ in north, east and up, respectively, it was excluded from the list of reference sites and the estimation was repeated. We subsequently estimated rates of the Helmert parameters (HP) $\dot{d}_{x,j}$, $\dot{d}_{y,j}$, $\dot{d}_{z,j}$ and $\dot{\alpha}_j$, $\dot{\beta}_j$, $\dot{\gamma}_j$ by fitting a deterministic model including offset, linear trend and annual signal to the time series of the HPs. Ideally, the linear rates of HPs would be similar for all ACs, indicating no systematic biases between the solutions on secular time scales. The resulting rates (Fig. 3) reveal a maximum magnitude equivalent to $0.45\,\mathrm{mm\,yr^{-1}}$ for $\dot{\alpha}$ of the TUD solution. The differences in $\dot{d}_z$ for all solutions are in the range of up to $0.4\,\mathrm{mm\,yr^{-1}}$, with the biggest difference between OSU and TUD. Since the HPs were estimated from a set of regionally distributed IGS sites, some HPs (e. g. $\boldsymbol{R}_x$ and $\boldsymbol{T}_y$) can not be independently resolved. Therefore, we applied the linear trends of the HPs on a defined grid covering our region of interest, resulting in point-wise velocities. We then transform the point-wise geocentric velocities to local, topocentric velocities (north, east, vertical), resulting in maps depicted in Fig. 3b, which allow for a comparison of the velocity patterns. The OSU and NEWC processings exhibit a similar pattern, dominated by the rate of translation in Z, resulting in a maximum magnitude of $0.15\,\mathrm{mm\,yr^{-1}}$ (NEWC) and $0.33\,\mathrm{mm\,yr^{-1}}$ (OSU) of local subsidence. The TUD pattern shows local vertical rates ranging from $0.27\,\mathrm{mm\,yr^{-1}}$ to $-0.10\,\mathrm{mm\,yr^{-1}}$, while the lateral velocities are well below $0.20\,\mathrm{mm\,yr^{-1}}$. The parameters $\dot{d}_x$, $\dot{d}_y$ and $\dot{\alpha}$ and $\dot{\beta}$ estimated by UTAS are somewhat larger, but cancel out for our region of interest, resulting in a small lateral deformation pattern with values well below $0.10\,\mathrm{mm\,yr^{-1}}$ and uplift rates with a maximum of $0.13\,\mathrm{mm\,yr^{-1}}$.

The differences in the observed patterns can be explained, at least in part, by the application of different reference frame realisation strategies. A maximum consistency to the ITRF is achieved when a globally, distributed set of IGS reference sites is used, as is the case for the processing of OSU and NEWC and inherently for the PPP solution of UTAS. Still, differences in the observed pattern are apparent and are in the same order of magnitude as differences to the TUD solution which relies on a reference frame realisation based on regionally distributed IGS sites. Considering the order of magnitude of the differences in the vertical rate pattern, a straightforward combination of the individual coordinate time series is prohibited to avoid introducing biases. Therefore, we decided to transform all four individual AC solutions using the the daily six HP to a common frame in order to minimise the systematic differences between the solutions.

3.2.2 Identification of systematically biased solutions

After we minimised the biases between the networks of the individual solutions on the longest time scales, we identified remaining systematic biases between the solutions on a site-by-site basis with a semi-automated procedure. For each site, we formed the median time series over the individual AC solutions for each local topocentric coordinate component (north, east and up) and computed the differences between each individual solution and the median time series. Sections of continuous time series or campaigns of episodic time series of individual solutions that showed differences larger than $10\,\mathrm{mm}$, $10\,\mathrm{mm}$ or $20\,\mathrm{mm}$ in north, east and up, respectively, were flagged. If the flagged solutions could be related to processing choices and could, therefore, be considered as systematically biased, the biased solutions were excluded from the subsequent combination

step. Examples for systematic biases are displayed in Fig. 4. The systematic bias for the UTAS solution (Fig. 4a) following an upgrade to the Septentrio PolaNt-x-MF antenna (IGS code: SEPPOLANT_X_MF) and Alertgeo Resolute receivers is evident for every upgraded POLENET station and therefore requires the exclusion of the UTAS solution after the upgrade. The TUD analysis included a correction for an antenna misalignment from true north, which is not considered by the other ACs. If the lateral antenna phase centre offsets provided with the igs14.atx file are significant and the antenna misalignment from true north is sufficiently large, the TUD solution shows biases in the lateral coordinate component relative to the other solutions (Fig. 4b). Sections of the TUD solutions showing the described biases were, therefore, excluded from the data combination.

3.2.3 Combining the individual coordinate time series

Finally, we combined the individual AC solutions to create the final data set. We implemented a site-wise combination approach by computing the weighted average over the ACs for each geocentric coordinate component:

$$x(t)_{combined} = \frac{\sum_{j=1}^{N} \sigma_{j,s}^2(t) \cdot x_j(t)}{N \cdot \sum_{j=1}^{N} \sigma_{j,s}^2(t)}, \tag{2}$$

with $\sigma_{j,s}^2$ the scaled variance and $x_j(t)$ the daily geocentric coordinate solution of the AC j. The uncertainties provided with the individual solutions do not provide a realistic measure of uncertainty for the daily coordinate solution. To obtain realistic uncertainty information on the estimated coordinates, error covariance information for the input products (orbits, clock corrections, tropospheric corrections) would be required to correctly propagate error information to the estimated parameters (e. g. station coordinates). The error information provided by each AC has, therefore, limited meaning in an absolute sense and is not comparable between the AC solutions, but they do contain information about the relative (internal) uncertainty of the solution of an AC. This imposes the necessity to scale the variances for each AC solution. The unscaled variances $\sigma_j^2(t)$ were scaled in such a way that the temporal mean over the scaled variances $\sigma_{j,s}^2(t)$ of AC j equals the repeatability (variance) of the residual coordinate time series $\sigma_{j,res}^2 = var[x_{j,res}(t)]$:

$$\sigma_{j,s}^2(t) = \sigma_j^2(t) \frac{\sigma_{j,res}^2}{\sigma_j^2}. \tag{3}$$

The advantage of this approach is twofold: First, the scaled variances are related to the repeatability of the residual coordinate time series and therefore have a physical, absolute meaning. Second, the coordinate time series of an AC showing less noise results in a smaller scaled variance and, consequently, higher weighting in the coordinate combination. A limitation of this approach results from the differing temporal coverage and sampling of the individual solutions of the non-stationary coordinate time series.

The required residual coordinate time series were formed by fitting and removing a deterministic trajectory model from the coordinate time series. The trajectory model contains linear trend, annual and semi-annual signal terms, and where needed post-seismic relaxation and a Heaviside step function and, thus, resembles a shortened version of the trajectory model described by

Bevis and Brown (2014):

$$x(t) = \sum_{i=0}^{n_p} p_i(t - t_R)^i + \sum_{i=1}^{n_J} b_j H(t - t_j) + \sum_{i=1}^{n_F} s_i \sin(\omega_i t) + c_i \cos(\omega_i t) + \qquad (4)$$

$$\sum_{i=1}^{n_T} e_i(1 - exp(1 - (t - t_i)/T_i)) + \sum_{j=1}^{n_L} a_j \log(1 + (t - t_j)/T_j).$$

We limit the polynomial degree to $n_P = 1$ and the seasonal harmonics to annual and semi-annual signals. Post-seismic defor-
mation terms were fitted for the sites BORC and DAL5. The automated identification of steps posed a difficult task (Gazeaux
et al., 2013). The limited number of sites within our study allowed for the manual (hand-picked) assessment of steps in the time
series. We indicated the time stamps of equipment changes, changes in the antenna eccentricity, occurrence of nearby earth-
quakes and the efforts of sealing antenna ground plates (see sec. 2.2). If a jump was apparent in one coordinate component,
steps were set up for all coordinate components. A full list of events potentially influencing coordinate trajectories is provided
with the final data product.

We omitted the seasonal and postseismic deformation terms for eGPS sites. Additionally, we introduced a jump between each
measurement campaign, removing inter-campaign biases. If the inter-campaign biases were not considered in the trajectory
model, the residual time series would contain intra-campaign noise and inter-campaign biases. The number of solved measure-
ment campaigns can vary between the AC solutions for eGPS sites. The AC solution which contained more campaigns would,
therefore, contain a higher number of inter-campaign biases (if the number of campaigns is larger than two), resulting in an
increased residual RMS. An AC solution would be downweighted in the combination (see Eq. 2) for solving more campaigns.
In a final step, we reduce the combined coordinate time series by the effect of the mean daily NTAL deformation. The compu-
tation of the NTAL time series follows the procedure outlined in section 3.1 for the NEWC processing.

3.3 Inference of time series of the Zenith Total Delay (ZTD)

The site-wise tropospheric delay in the form of the zenith total delay (ZTD) were estimated together with the daily station
coordinates by each AC as described in sec. 3.1. We provide the site-wise time series of ZTD estimates as an auxiliary data
set (Buchta et al., 2024e). The TUD, OSU and NEWC ACs parameterise the ZTD as piece-wise linear functions, leading to
duplicate estimates at the day boundaries. To form a continuous time series, the estimates for each AC were averaged at the
day boundaries. The high rate UTAS solution was downsampled by forming hourly averages. Here, we decided against the
combination of ZTD results and provide the individual AC solutions instead.

4 Results

4.1 Combined coordinate time series

As the major product we provide the combined coordinate time series for 286 bedrock sites in Antarctica (Buchta et al., 2024b).
The individual ACs provided solutions for 286 (TUD), 286 (UTAS), 258 (OSU), and 270 (NEWC) sites. The differences in the

Table 1. The median of the repeatability (RMS) derived from residual coordinate time series for the north, east and up coordinate component for a selection of 29 stable continuous sites.

	north RMS [mm]	east RMS [mm]	up RMS [mm]
TUD	1.9	1.5	5.4
OSU	1.8	1.2	4.1
UTAS	1.9	1.6	6.3
NEWC	1.4	1.2	5.6
combination	1.5	1.1	4.5
combination (NTAL removed)	1.3	1.1	3.6

380   number of solutions are due to different approaches and thresholds concerning the quality or completeness of the observational data. The combination leads to a small increase in the total number of daily solutions. The comparison of the number of daily solutions per site between the combination and the individual solution with the most solutions results in a mean increase of $0.3\,\%$. The resulting mean time base of the combined product is 10.5 years. Fig. 5 shows an example coordinate time series comprising both the individual and combined solutions. To assess the repeatability and noise characteristics of the individual

385   and the combined solutions, we analysed the coordinate time series of 29 stable cGPS sites. These sites were selected to cover a time span of at least six years, to have no reported snow intrusions, are not subject to other external disturbances, and are well distributed over the Antarctic continent (see Fig. 6). First, residual time series were formed by fitting and subtracting a deterministic model (Eq. 4) from the time series (see Fig. 5 for an example time series). Post-seismic deformation terms were neglected for the selected sites. Steps were consistently introduced for all ACs and the combined time series. The repeatability

390   of the coordinate time series is then described by the derived RMS over the residual time series. Tab. 1 displays the median RMS for each AC and the combined solutions. The NEWC solution shows the lowest RMS for the lateral components with a median RMS of 1.4 and $1.2\,\text{mm}$ for north and east, respectively. The solution of OSU reaches the smallest median RMS for the vertical coordinate component with $4.1\,\text{mm}$. The repeatability for the TUD and UTAS solutions show higher values for the north and up components. The RMS values of the combined time series resemble the lowest RMS of the best-performing individual

395   solutions for the lateral components with -0.1, $-0.1\,\text{mm}$ for north and east respectively, compared to the best performing individual solution. The RMS for the vertical component is found to be $0.4\,\text{mm}$ larger than that of the OSU solution.

   To further characterise the spectral properties of the residual time series we calculated the Lomb-Scargle periodogram (LSP), a representation of the power-spectral density for non-uniformly sampled data (VanderPlas, 2018). We used un-normalized LSPs where the power spectral density takes values similar to FFT analysis, differing by a factor of two in the case of a complete

400   time series. LSPs were computed for all sites and each coordinate component for each AC and for the combined solutions. Subsequently, the median LSP was formed over all 29 sites, allowing for the direct comparison between the solutions (Fig. 7). Firstly, the periodograms confirm the generally lower noise levels of the lateral coordinate components of the NEWC and

OSU solutions compared to the TUD and UTAS solutions, especially at high frequencies. All solutions follow the well-known power-law like behavior of GPS coordinate time series, close to flicker noise (spectral index equals -1) and white noise for very high frequencies (Liu et al., 2018; King et al., 2022). Differences between the solutions become apparent for distinct frequencies. Dominant peaks are visible for the, otherwise very low noise, periodograms of the NEWC (north, east, up) and OSU (east) solutions at the fortnightly periods of 13.63 and $14.16\,\mathrm{d}$, possibly resulting from "direct" and "indirect/aliased" errors in tidal models (Ray et al., 2013). Smaller peaks are visible at $9.4\,\mathrm{d}$ for UTAS (up) and $9.14\,\mathrm{d}$ for NEWC (up), also resulting from direct and indirect errors in tidal models, respectively. At lower frequencies distinct peaks at harmonics of the GPS draconitic year ($351\,\mathrm{d}$) are apparent (Ray et al., 2008). The combined time series reveals reduced amplitudes for the spurious signals at high frequencies, whereas the draconitic harmonics remain at high amplitudes.

Combining the individual solutions, as described in section 3.2.3, has several advantages over the individual solutions: the repeatability is similar to the best-performing single AC solution, the amplitudes of high-frequency interfering signals have been reduced, and the overall spatio-temporal coverage has been increased.

The effect of NTAL induced deformations was removed from the combined coordinate time series to form infer the final data set. A number of studies discussed the influence of NTAL effects on GPS time series, leading to a reduction in the amplitude of annual signals and the residual RMS depending on the site location (Männel et al., 2019; Mémin et al., 2020). For the selection of stable sites we find a mean reduction of the residual RMS of 0.2, 0.0 and $0.9\,\mathrm{mm}$ (see Tab. 1) and a mean reduction of the annual amplitude of 0.1, 0.0 and $0.6\,\mathrm{mm}$ for north, east and vertical, respectively. The maximum reduction of the vertical annual amplitude was found for the site FALL with $2.5\,\mathrm{mm}$. An increase in the annual amplitude was identified for sites in Dronning Maud Land, with a maximum of $1.6\,\mathrm{mm}$ for the site ABOA.

We realised the terrestrial reference frame IGb14 using a regional selection of reference sites for the individual AC solutions (see section 3.2.3). As shown by Legrand et al. (2010), using a sparse set of regionally distributed reference sites can introduce a (secular) bias in the coordinate solutions. This adds to the uncertainty of the reference frame itself which shows a secular bias of $0.2\,\mathrm{mm}\,\mathrm{yr}^{-1}$ in the polar axis when comparing ITRF2014 to ITRF2020 (Altamimi et al., 2023). Uncertainties in the reference frame realization, especially in the Z-axis, map onto the uncertainty in the local vertical coordinate component of sites in the polar regions and must be taken into account when using them for geodynamic studies (e.g. GIA).

4.2 Comparison to the data set of the Nevada Geodetic Laboratory (NGL)

In order to evaluate our results using an independent solution, we compared and validated the results of our GIANT-REGAIN (GR) combined solution with the data products of the Nevada Geodetic Laboratory (NGL), University of Reno (Blewitt et al., 2018). Their publicly available "living data set" consists of coordinate time series of more than $17{,}000$ globally distributed GPS stations with more than $10{,}000$ stations updated every week. The NGL processing employs the PPP processing strategy of the GipsyX software, which provides a computationally efficient method to process an immense amount of data. The processing uses GPS observations only, and JPL orbit and clock products (Earth orientation parameters, satellite clocks and ephemerides). The coordinate solutions are realised in the IGS14 reference frame. We refer to web resources[3] for further details on the NGL

---

[3] http://geodesy.unr.edu/gps/ngl.acn.txt

processing setup. In their solutions, the critical metadata (including antenna types and heights) are extracted from the header section of RINEX observation files.

To compare the data sets we selected 157 sites (55% of the GR data set) available in both data sets and downloaded the final, cleaned NGL time series of geocentric coordinates (Fig. 8). For this comparison, neither data set was corrected for NTAL

440 deformation.

To check the consistency of the data sets, we compared the linear rates of coordinate change derived from both data sets. For this purpose, the NGL data set is limited to the GIANT-REGAIN period from 1995-001 to 2021-365. Further we limited the analysed stations to those that have an observation span of at least three years in both data sets, resulting in a selection of 143 sites. We used the local topocentric coordinate representation (north, east, up) for the analysis. The Hector software package

445 v1.9 (Bos et al., 2013) was used to fit a deterministic model (Eq. 4) to the time series, while assuming a white and flicker noise stochastic model. The deterministic model is limited to a linear trend and potential offsets for eGPS sites. We extracted information on discontinuities for the NGL data set from the provided master step file data base[4]. Steps in the GR data set are consistent with the ones used in Sec. 3.2.3.

Sites with large trend differences exceeding $10 \, \mathrm{mm \, yr^{-1}}$ in either north, east or up were considered outliers and excluded from

450 the subsequent analysis. Five sites exceeded this threshold: MBL3, SLTR, VL06, VL20 and VLHG. The large differences can be explained by different assumptions regarding antenna heights and different identification of jumps in the GR and NGL data sets. The distribution of trend differences (GR - NGL) for the remaining stations reveals a high level of consistency (Fig. 9). The mean differences and standard deviations can be considered small with $0.1 \pm 0.6 \, \mathrm{mm \, yr^{-1}}$, $0.0 \pm 0.8 \, \mathrm{mm \, yr^{-1}}$ and $0.2 \pm 1.1 \, \mathrm{mm \, yr^{-1}}$ for north, east and up, respectively. The estimated rates are sensitive to the assumed steps in the

455 deterministic models. We repeated the estimation of the trends for the NGL data set, but introduced step information consistent with the GR data set. The increased consistency of the deterministic models leads to a further reduction of the trend differences for the lateral components to $0.0 \pm 0.4 \, \mathrm{mm \, yr^{-1}}$ and $0.0 \pm 0.5 \, \mathrm{mm \, yr^{-1}}$ for the north and east components, respectively. The differences of estimated rates reflect differences a user would obtain using either data set for the defined time span. They do not solely describe differences that result from the different processing strategies. Individual site time series may have different

460 temporal coverage for either data set and, therefore, be affected differently by nonlinear loading variations (Koulali et al., 2022; King et al., 2022).

The NGL data set originates from a highly-automated processing and retrieves the necessary metadata from the header section of the observational RINEX file (Blewitt et al., 2018) which can be prone to errors. The NGL data set provides antenna heights together with the coordinate time series, enabling the comparison with the revised metadata information of the GR data set.

465 The comparison reveals different antenna heights for 57 sites and antenna height differences greater than $4 \, \mathrm{mm}$ (approximate noise level of the up component, see table 1) for 43 sites, equaling 36% and 27% of sites respectively. Differences in the antenna heights do not necessarily result in differences in estimated trajectory models, e.g. if the antenna height difference is constant for the whole observation time or between estimated steps. We quantify the impact of the improved antenna height

---

[4]http://geodesy.unr.edu/NGLStationPages/steps.txt

information, by modifying the NGL time series of the up component $u_{NGL}(t)$ for the 57 sites as:

$$u_{NGL}^{mod}(t) = u(t)_{NGL} + H_{NGL}(t) - H_{GR}(t), \tag{5}$$

with $H_{NGL}(t)$ the antenna height provided by NGL at time t and $H_{GR}(t)$ the antenna height provided by the GR data set at time t. We detrended $u_{NGL}(t)$ and $u_{NGL}^{mod}(t)$ and computed the residual RMS for all 57 sites. The mean RMS shows a reduction from $21.3\,\text{mm}$ to $8.5\,\text{mm}$ and the median RMS from $9.1\,\text{mm}$ to $7.9\,\text{mm}$. The RMS reduction results from the correction of outliers and the reduction of steps associated with antenna changes. Example coordinate time series displaying the effect of corrected antenna heights are given in the supporting material.

5 Conclusions

We collected and evaluated observational data and station metadata for 286 GPS sites in Antarctica from 1995 to 2021. The processing of the data was carried out by four analysis centres. This allowed us to maximise the temporal and spatial coverage of our data set and to identify possible biases in individual solutions. In this way, we were able to generate a consistent combined data set of coordinate time series. Compared to the data set provided by the Nevada Geodetic Laboratory (NGL), which contains the largest number of GNSS sites in Antarctica to date, we were able to increase the spatial coverage, especially in East Antarctica. In some regions, such as Victoria Land and the Antarctic Peninsula, the comparably high density of stations could be increased even more. Our revised station metadata decreases the number of artefacts (e.g. outliers and jumps) in the coordinate time series and provides the basis for a reliable analysis of episodic (eGPS) sites.

The main product – consistent GPS coordinate time series – is supplemented by the data sets of time series of the zenith total delay as well as the station metadata in the form of IGS log files and a station event list. The latter is intended to serve as a possible starting point for analysing and interpreting the coordinate trajectory, as it contains information on equipment changes, nearby earthquakes and measures taken to mitigate snow contamination of the GPS antennas.

The inferred consistent coordinate time series will advance the investigation of various geodynamic effects on different time scales. Derived linear rates may be employed to examine plate motion or to validate and constrain models of GIA. The enhanced spatial and temporal coverage of this data set will allow to assess GIA models more rigorously than previously possible. This pertains to the spatial coverage, notably in East Antarctica, as well as the augmented station density in regions of increased lateral gradients in the vertical uplift rates, exemplified by the northern Antarctic Peninsula (Koulali et al., 2022) and the Amundsen Sea region (Barletta et al., 2018). However, the isolation of the GIA signal, in particular in the vertical component, requires the removal of the instantaneous (elastic) deformation caused by the present-day mass change, i.e. superimposed loading due to SMB and changes in ice dynamics (Hattori et al., 2021; Koulali et al., 2022; King et al., 2022), which is not within the scope of the study. Therefore, we do not provide a product of secular rates from the coordinate time series. However, to demonstrate the potential of the data set, we derive linear rates for all sites with a time base larger than $2.5\,\text{yr}$ and at least ten data points (Fig. 10), using the trajectory models described in Sec. 3.2.3.

Furthermore, this data set, especially the derived station metadata, will serve as a baseline for anticipated future reprocessing

efforts, which could then take into account up-to-date ITRF realisation and associated conventions, extend the coordinate time series of existing stations and include new GPS stations in the data set. The compilation of all available GPS data provides an unprecedented insight into solid Earth deformation in Antarctica. The comprehensive overview (e.g. Fig. 8) highlights gaps in GPS coverage and will be used to plan future station deployments to further improve coverage and maintenance of the geodetic infrastructure.

6 Code availability

The GNSS analysis software used is available from the relevant research groups. Parallel.GAMIT is available at https://github.com/demiangomez/Parallel.GAMIT.

7 Data availability

The product inferred by this project is available at the PANGAEA repository (https://doi.pangaea.de/10.1594/PANGAEA.967515) (Buchta et al., 2024a) as a data set collection and comprises four individual data sets: the combined coordinate time series (https://doi.pangaea.de/10.1594/PANGAEA.967516) (Buchta et al., 2024b), the time series of the tropospheric Zenith Total Delays (ZTD) from the individual analysis centres processing (https://doi.pangaea.de/10.1594/PANGAEA.967529) (Buchta et al., 2024e), the station information in the form of IGS log files (https://doi.pangaea.de/10.1594/PANGAEA.967532) (Buchta et al., 2024d) and a list of events (https://doi.pangaea.de/10.1594/PANGAEA.967533) (Buchta et al., 2024c), which can be employed in conjunction with the coordinate time series data to analyse the coordinate trajectory. The data sources of publicly available observational data are listed in Tab. S1 in the supplementary material.

Author contributions. MS and MAK conceptualized the study. CK, EB, EK, MS, MAK, PJC, PB and TW were involved in the collection and compilation of the observational data and station metadata. EB, MAK, DG and AK conducted the individual GPS processing. EB performed the data combination and comparison to the external data set. EB wrote the majority of the main text, and compiled all figures, except Fig. 10. All authors contributed to the writing and editing of the manuscript.

Competing interests. The authors declare that they have no conflict of interest.

Acknowledgements. This study was endorsed by the Scientific Committee on Antarctic Research (SCAR), and especially by the SCAR Expert Group "Geodetic Infrastructure in Antarctica" (GIANT). We would like to thank all colleagues and institutions who have supported GIANT for many years. We extend our gratitude to all institutions and operators who have contributed GNSS data and detailed station information within the context of the GIANT-REGAIN project: POLENET and UKANET initiative and their respective contributing partners,

Alfred Wegener Institute Helmholtz Centre for Polar and Marine Research (AWI), Australian National University (ANU), Finnish Antarctic Research Program (FINNARP), Geoscience Australia (GA), Hartebeesthoek Radio Astronomy Observatory (South Africa), Instituto Antártico Argentino, Instituto Geográfico Militar de Chile, Royal Institute of Technology (KTH, Sweden), Norwegian Polar Institute, Geodetic

530   Reference System for the Americas (SIRGAS), EarthScope (formerly UNAVCO), University of Architecture, Civil Engineering and Geodesy (UACEG, Bulgaria), University of Luxembourg, the University of Memphis (USA), the University of Modena and Reggio Emilia (Italy), and the University of Texas at Austin (USA). We would like to express our gratitude to the International GNSS Service (IGS) and the associated analysis centres and data centres for providing high-quality GNSS products. We thank NASA JPL for the provision of GIPSY and their orbit and clock products. The establishment, operation and maintenance of the GNSS sites in Antarctica would not have been possible without

535   the huge logistic and personnel support by a large number of national Antarctic programs and institutions which we cannot list in full here. Their dedication and support is greatly acknowledged. NEWC especially thanks the British Antarctic Survey (BAS).

PYGMT, the Python API for Generic Mappping Tools software v6 (Wessel et al., 2019) was used to generate Figs. 2, 3, 6, 8, 9 and 10, and QGIS and Quantarctica v3.2 (Matsuoka et al., 2021) were used to generate Fig. 1.

The work of MAK was supported by the ARC Australian Centre for Excellence in Antarctic Science (Project ID SR200100008) and the

540   Australian Government's Australian Antarctic Program (Projects 4318 and 4547). The work of AK and PJC has been supported by UK Natural Environment Research Council (NERC) grants NE/K004085/1 and NE/R002029/1. The authors are grateful to the two reviewers whose constructive and insightful comments which were of great help to improve the manuscript and update the provided data set.

References

Altamimi, Z., Rebischung, P., Métivier, L., and Collilieux, X.: ITRF2014: A new release of the International Terrestrial Reference Frame modeling nonlinear station motions, Journal of Geophysical Research: Solid Earth, 121, 6109–6131, https://doi.org/10.1002/2016JB013098, 2016.

Altamimi, Z., Rebischung, P., Collilieux, X., Métivier, L., and Chanard, K.: ITRF2020: an augmented reference frame refining the modeling of nonlinear station motions, Journal of Geodesy, 97, 47, https://doi.org/10.1007/s00190-023-01738-w, 2023.

Andrei, C.-O., Lahtinen, S., Nordman, M., Näränen, J., Koivula, H., Poutanen, M., and Hyyppä, J.: GPS Time Series Analysis from Aboa the Finnish Antarctic Research Station, Remote Sensing, 10, https://doi.org/10.3390/rs10121937, 2018.

Argus, D. F., Blewitt, G., Peltier, W. R., and Kreemer, C.: Rise of the Ellsworth mountains and parts of the East Antarctic coast observed with GPS, Geophysical Research Letters, 38, https://doi.org/10.1029/2011GL048025, 2011.

Argus, D. F., Peltier, W. R., Drummond, R., and Moore, A. W.: The Antarctica component of postglacial rebound model ICE-6G_C (VM5a) based on GPS positioning, exposure age dating of ice thicknesses, and relative sea level histories, Geophysical Journal International, 198, 537–563, https://doi.org/10.1093/gji/ggu140, 2014.

Bar-Sever, Y. E., Kroger, P. M., and Borjesson, J. A.: Estimating horizontal gradients of tropospheric path delay with a single GPS receiver, Journal of Geophysical Research: Solid Earth, 103, 5019–5035, https://doi.org/https://doi.org/10.1029/97JB03534, 1998.

Barletta, V. R., Bevis, M., Smith, B. E., Wilson, T., Brown, A., Bordoni, A., Willis, M., Khan, S. A., Rovira-Navarro, M., Dalziel, I., Smalley, R., Kendrick, E., Konfal, S., Caccamise, D. J., Aster, R. C., Nyblade, A., and Wiens, D. A.: Observed rapid bedrock uplift in Amundsen Sea Embayment promotes ice-sheet stability, Science, 360, 1335–1339, https://doi.org/10.1126/science.aao1447, 2018.

Bertiger, W., Desai, S. D., Haines, B., Harvey, N., Moore, A. W., Owen, S., and Weiss, J. P.: Single receiver phase ambiguity resolution with GPS data, Journal of Geodesy, 84, 327–337, https://doi.org/10.1007/s00190-010-0371-9, 2010.

Bevis, M. and Brown, A.: Trajectory models and reference frames for crustal motion geodesy, Journal of Geodesy, 88, 283–311, https://doi.org/10.1007/s00190-013-0685-5, 2014.

Bevis, M., Kendrick, E., Smalley Jr., R., Dalziel, I., Caccamise, D., Sasgen, I., Helsen, M., Taylor, F. W., Zhou, H., Brown, A., Raleigh, D., Willis, M., Wilson, T., and Konfal, S.: Geodetic measurements of vertical crustal velocity in West Antarctica and the implications for ice mass balance, Geochemistry, Geophysics, Geosystems, 10, https://doi.org/10.1029/2009GC002642, 2009.

Blewitt, G., Hammond, W. C., and Kreemer, C.: Harnessing the GPS data explosion for interdisciplinary science, EOS, 99, https://doi.org/10.1029/2018EO104623, 2018.

Boehm, J., Werl, B., and Schuh, H.: Troposphere mapping functions for GPS and very long baseline interferometry from European Centre for Medium-Range Weather Forecasts operational analysis data, Journal of geophysical research: solid earth, 111, 2006.

Bos, M. S., Fernandes, R. M. S., Williams, S. D. P., and Bastos, L.: Fast error analysis of continuous GNSS observations with missing data, Journal of Geodesy, 87, 351–360, https://doi.org/10.1007/s00190-012-0605-0, 2013.

Bouin, M.-N. and Vigny, C.: New constraints on Antarctic plate motion and deformation from GPS data, Journal of Geophysical Research: Solid Earth, 105, 28 279–28 293, https://doi.org/10.1029/2000JB900285, 2000.

Buchta, E., Scheinert, M., King, M. A., Wilson, T., Clarke, P. J., Gómez, D., Kendrick, E., Knöfel, C., and Koulali, A.: Daily coordinate time series for GPS stations on bedrock for Antarctica and the sub Antarctic sector, 1995–2021, reprocessed by the GIANT-REGAIN project, PANGAEA [data set], https://doi.org/10.1594/PANGAEA.967515, 2024a.

Buchta, E., Scheinert, M., King, M. A., Wilson, T., Clarke, P. J., Gómez, D., Kendrick, E., Knöfel, C., and Koulali, A.: Daily co-ordinate time series for GPS stations on bedrock for Antarctica and the sub Antarctic sector, 1995–2021, PANGAEA [data set], doi.pangaea.de/10.1594/PANGAEA.967516, 2024b.

Buchta, E., Scheinert, M., King, M. A., Wilson, T., Clarke, P. J., Gómez, D., Kendrick, E., Knöfel, C., and Koulali, A.: Event list for GPS stations on bedrock for Antarctica and the sub antarctic sector, 1995–2021, PANGAEA [data set], https://doi.pangaea.de/10.1594/PANGAEA.967533, 2024c.

Buchta, E., Scheinert, M., King, M. A., Wilson, T., Clarke, P. J., Gómez, D., Kendrick, E., Knöfel, C., and Koulali, A.: Sta-tion information for GPS stations on bedrock for Antarctica and the sub Antarctic sector, 1995–2021, PANGAEA [data set], https://doi.pangaea.de/10.1594/PANGAEA.967532, 2024d.

Buchta, E., Scheinert, M., King, M. A., Wilson, T., Clarke, P. J., Gómez, D., Kendrick, E., Knöfel, C., and Koulali, A.: Sub-daily zenith total delay time series for GPS stations on bedrock for Antarctica and the sub Antarctic sector, 1995–2021, PANGAEA [data set], https://doi.pangaea.de/10.1594/PANGAEA.967529, 2024e.

Burton-Johnson, A., Black, M., Fretwell, P. T., and Kaluza-Gilbert, J.: An automated methodology for differentiating rock from snow, clouds and sea in Antarctica from Landsat 8 imagery: a new rock outcrop map and area estimation for the entire Antarctic continent, The Cryosphere, 10, 1665–1677, https://doi.org/10.5194/tc-10-1665-2016, 2016.

Busch, P., Scheinert, M., and Knoefel, C.: GNSS measurements in West Antarctica to reconcile glacial-isostatic adjustment. Presented at the IAG/SCAR-SERCE Workshop on Glacial Isostatic Adjustment and Elastic Deformationn, 5 – 7 September 2017, Reykjavik, Iceland, 2017.

Dach, R., Andritsch, F., Arnold, D., Bertone, S., Fridez, P., Jäggi, A., Jean, Y., Maier, A., Mervart, L., Meyer, U., Orliac, E., Geist, E., Prange, L., Scaramuzza, S., Schaer, S., Sidorov, D., Susnik, A., Villiger, A., Walser, P., and Thaller, D.: Bernese GNSS Software Version 5.2, https://doi.org/10.7892/boris.72297, 2015.

Dietrich, R., Dach, R., Engelhardt, G., Ihde, J., Korth, W., Kutterer, H.-J., Lindner, K., Mayer, M., Menge, F., Miller, H., Müller, C., Niemeier, W., Perlt, J., Pohl, M., Salbach, H., Schenke, H.-W., Schöne, T., Seeber, G., Veit, A., and Völksen, C.: ITRF coordinates and plate velocities from repeated GPS campaigns in Antarctica – an analysis based on different individual solutions, Journal of Geodesy, 74, 756–766, https://doi.org/10.1007/s001900000147, 2001.

Dietrich, R., Rülke, A., Ihde, J., Lindner, K., Miller, H., Niemeier, W., Schenke, H.-W., and Seeber, G.: Plate kinematics and deformation sta-tus of the Antarctic Peninsula based on GPS, Global and Planetary Change, 42, 313–321, https://doi.org/10.1016/j.gloplacha.2003.12.003, 2004.

Dong, D., Herring, T. A., and King, R. W.: Estimating regional deformation from a combination of space and terrestrial geodetic data, Journal of Geodesy, 72, 200–214, https://doi.org/10.1007/s001900050161, 1998.

Donnellan, A. and Luyendyk, B. P.: GPS evidence for a coherent Antarctic plate and for postglacial rebound in Marie Byrd Land, Global and Planetary Change, 42, 305–311, https://doi.org/10.1016/j.gloplacha.2004.02.006, 2004.

Fu, Y., Freymueller, J. T., and van Dam, T.: The effect of using inconsistent ocean tidal loading models on GPS coordinate solutions, Journal of Geodesy, 86, 409–421, https://doi.org/10.1007/s00190-011-0528-1, 2012.

Gazeaux, J., Williams, S., King, M., Bos, M., Dach, R., Deo, M., Moore, A. W., Ostini, L., Petrie, E., Roggero, M., Teferle, F. N., Olivares, G., and Webb, F. H.: Detecting offsets in GPS time series: First results from the detection of offsets in GPS experiment, Journal of Geophysical Research: Solid Earth, 118, 2397–2407, https://doi.org/https://doi.org/10.1002/jgrb.50152, 2013.

Gómez, D. D., Bevis, M. G., and Caccamise, D. J.: Maximizing the consistency between regional and global reference frames utilizing inheritance of seasonal displacement parameters, Journal of Geodesy, 96, 9, https://doi.org/10.1007/s00190-022-01594-0, 2022.

Grapenthin, R., Kyle, P., Aster, R. C., Angarita, M., Wilson, T., and Chaput, J.: Deformation at the open-vent Erebus volcano, Antarctica, from more than 20 years of GNSS observations, Journal of Volcanology and Geothermal Research, 432, 107 703, https://doi.org/10.1016/j.jvolgeores.2022.107703, 2022.

Groh, A. and Horwath, M.: Antarctic Ice Mass Change Products from GRACE/GRACE-FO Using Tailored Sensitivity Kernels, Remote Sensing, 13, https://www.mdpi.com/2072-4292/13/9/1736, 2021.

Groh, A., Ewert, H., Scheinert, M., Fritsche, M., Rülke, A., Richter, A., Rosenau, R., and Dietrich, R.: An investigation of Glacial Isostatic Adjustment over the Amundsen Sea sector, West Antarctica, Global and Planetary Change, 98-99, 45–53, https://doi.org/10.1016/j.gloplacha.2012.08.001, 2012.

Hattori, A., Aoyama, Y., Okuno, J., and Doi, K.: GNSS Observations of GIA-Induced Crustal Deformation in Lützow-Holm Bay, East Antarctica, Geophysical Research Letters, 48, e2021GL093 479, https://doi.org/10.1029/2021GL093479, 2021.

Herring, T. A., Melbourne, T. I., Murray, M. H., Floyd, M. A., Szeliga, W. M., King, R. W., Phillips, D. A., Puskas, C. M., Santillan, M., and Wang, L.: Plate Boundary Observatory and related networks: GPS data analysis methods and geodetic products, Reviews of Geophysics, 54, 759–808, https://doi.org/10.1002/2016RG000529, 2016.

Johnston, G., Riddell, A., and Hausler, G.: The International GNSS Service, pp. 967–982, Springer International Publishing, Cham, https://doi.org/10.1007/978-3-319-42928-1_33, 2017.

Kedar, S., Hajj, G. A., Wilson, B. D., and Heflin, M. B.: The effect of the second order GPS ionospheric correction on receiver positions, Geophysical Research Letters, 30, https://doi.org/10.1029/2003GL017639, 2003.

King, M. A. and Santamaría-Gómez, A.: Ongoing deformation of Antarctica following recent Great Earthquakes, Geophysical Research Letters, 43, 1918–1927, https://doi.org/10.1002/2016GL067773, 2016.

King, M. A., Penna, N. T., Clarke, P. J., and King, E. C.: Validation of ocean tide models around Antarctica using onshore GPS and gravity data, Journal of Geophysical Research: Solid Earth, 110, https://doi.org/10.1029/2004JB003390, 2005.

King, M. A., Altamimi, Z., Boehm, J., Bos, M., Dach, R., Elosegui, P., Fund, F., Hernández-Pajares, M., Lavallee, D., Mendes Cerveira, P. J., Penna, N., Riva, R. E. M., Steigenberger, P., van Dam, T., Vittuari, L., Williams, S., and Willis, P.: Improved Constraints on Models of Glacial Isostatic Adjustment: A Review of the Contribution of Ground-Based Geodetic Observations, Surveys in Geophysics, 31, 465–507, https://doi.org/10.1007/s10712-010-9100-4, 2010.

King, M. A., Bingham, R. J., Moore, P., Whitehouse, P. L., Bentley, M. J., and Milne, G. A.: Lower satellite-gravimetry estimates of Antarctic sea-level contribution, Nature, 491, 586–589, https://doi.org/10.1038/nature11621, 2012.

King, M. A., Whitehouse, P., and Clarke, P.: CAPGIA - West Antarctica Continuous Network, The GAGE Facility operated by EarthScope Consortium, GPS/GNSS Observations (Aggregation of Multiple Datasets), https://doi.org/10.7283/T56Q1VN5, 2013.

King, M. A., Watson, C. S., and White, D.: GPS Rates of Vertical Bedrock Motion Suggest Late Holocene Ice-Sheet Readvance in a Critical Sector of East Antarctica, Geophysical Research Letters, 49, https://doi.org/10.1029/2021GL097232, 2022.

Konfal, S., Kendrick, E., Saddler, D., Wilson, T., and Bevis, M.: Crustal velocity solutions in polar environments: GPS position errors caused by ice in antennas, in: SCAR Open Science Conference, Kuala Lumpur, Malaysia, 2016.

Kouba, J.: Implementation and testing of the gridded Vienna Mapping Function 1 (VMF1), Journal of Geodesy, 82, 193–205, https://doi.org/10.1007/s00190-007-0170-0, 2008.

Koulali, A. and Clarke, P. J.: Effect of antenna snow intrusion on vertical GPS position time series in Antarctica, Journal of Geodesy, 94, 101, https://doi.org/10.1007/s00190-020-01403-6, 2020.

Koulali, A., Whitehouse, P. L., Clarke, P. J., van den Broeke, M. R., Nield, G. A., King, M. A., Bentley, M. J., Wouters, B., and Wilson, T.: GPS-Observed Elastic Deformation Due to Surface Mass Balance Variability in the Southern Antarctic Peninsula, Geophysical Research Letters, 49, e2021GL097 109, https://doi.org/10.1029/2021GL097109, 2022.

Landskron, D. and Böhm, J.: VMF3/GPT3: refined discrete and empirical troposphere mapping functions, Journal of Geodesy, 92, 349–360, https://doi.org/10.1007/s00190-017-1066-2, 2018.

Legrand, J., Bergeot, N., Bruyninx, C., Wöppelmann, G., Bouin, M.-N., and Altamimi, Z.: Impact of regional reference frame definition on geodynamic interpretations, Journal of Geodynamics, 49, 116–122, https://doi.org/https://doi.org/10.1016/j.jog.2009.10.002, 2010.

Li, W., Li, F., Shum, C., Shu, C., Ming, F., Zhang, S., Zhang, Q., and Chen, W.: Assessment of Contemporary Antarctic GIA Models Using High-Precision GPS Time Series, Remote Sensing, 14, https://doi.org/10.3390/rs14051070, 2022.

Liu, B., King, M., and Dai, W.: Common mode error in Antarctic GPS coordinate time-series on its effect on bedrock-uplift estimates, Geophysical Journal International, 214, 1652–1664, https://doi.org/10.1093/gji/ggy217, 2018.

Luzum, B. and Petit, G.: The IERS Conventions (2010): reference systems and new models, Proceedings of the International Astronomical Union, 10, 227–228, https://doi.org/10.1017/S1743921314005535, 2012.

Lyard, F. H., Allain, D. J., Cancet, M., Carrère, L., and Picot, N.: FES2014 global ocean tide atlas: design and performance, Ocean Science, 17, 615–649, https://doi.org/10.5194/os-17-615-2021, 2021.

Männel, B., Dobslaw, H., Dill, R., Glaser, S., Balidakis, K., Thomas, M., and Schuh, H.: Correcting surface loading at the observation level: impact on global GNSS and VLBI station networks, Journal of Geodesy, 93, 2003–2017, https://doi.org/10.1007/s00190-019-01298-y, 2019.

Martín-Español, A., King, M. A., Zammit-Mangion, A., Andrews, S. B., Moore, P., and Bamber, J. L.: An assessment of forward and inverse GIA solutions for Antarctica, Journal of Geophysical Research: Solid Earth, 121, 6947–6965, https://doi.org/10.1002/2016JB013154, 2016.

Matsuoka, K., Skoglund, A., Roth, G., de Pomereu, J., Griffiths, H., Headland, R., Herried, B., Katsumata, K., Le Brocq, A., Licht, K., Morgan, F., Neff, P. D., Ritz, C., Scheinert, M., Tamura, T., Van de Putte, A., van den Broeke, M., von Deschwanden, A., Deschamps-Berger, C., Van Liefferinge, B., Tronstad, S., and Melvær, Y.: Quantarctica, an integrated mapping environment for Antarctica, the Southern Ocean, and sub-Antarctic islands, Environmental Modelling & Software, 140, 105 015, https://doi.org/10.1016/j.envsoft.2021.105015, 2021.

Mémin, A., Boy, J.-P., and Santamaría-Gómez, A.: Correcting GPS measurements for non-tidal loading, GPS Solutions, 24, 45, https://doi.org/10.1007/s10291-020-0959-3, 2020.

Nield, G. A., Barletta, V. R., Bordoni, A., King, M. A., Whitehouse, P. L., Clarke, P. J., Domack, E., Scambos, T. A., and Berthier, E.: Rapid bedrock uplift in the Antarctic Peninsula explained by viscoelastic response to recent ice unloading, Earth and Planetary Science Letters, 397, 32–41, https://doi.org/10.1016/j.epsl.2014.04.019, 2014.

Nield, G. A., King, M. A., Koulali, A., and Samrat, N.: Postseismic Deformation in the Northern Antarctic Peninsula Following the 2003 and 2013 Scotia Sea Earthquakes, Journal of Geophysical Research: Solid Earth, 128, e2023JB026 685, https://doi.org/10.1029/2023JB026685, 2023.

Otosaka, I. N., Shepherd, A., Ivins, E. R., Schlegel, N.-J., Amory, C., van den Broeke, M. R., Horwath, M., Joughin, I., King, M. D., Krinner, G., Nowicki, S., Payne, A. J., Rignot, E., Scambos, T., Simon, K. M., Smith, B. E., Sørensen, L. S., Velicogna, I., Whitehouse, P. L., A,

G., Agosta, C., Ahlstrøm, A. P., Blazquez, A., Colgan, W., Engdahl, M. E., Fettweis, X., Forsberg, R., Gallée, H., Gardner, A., Gilbert, L., Gourmelen, N., Groh, A., Gunter, B. C., Harig, C., Helm, V., Khan, S. A., Kittel, C., Konrad, H., Langen, P. L., Lecavalier, B. S., Liang, C.-C., Loomis, B. D., McMillan, M., Melini, D., Mernild, S. H., Mottram, R., Mouginot, J., Nilsson, J., Noël, B., Pattle, M. E., Peltier, W. R., Pie, N., Roca, M., Sasgen, I., Save, H. V., Seo, K.-W., Scheuchl, B., Schrama, E. J. O., Schröder, L., Simonsen, S. B., Slater, T., Spada, G.,

695   Sutterley, T. C., Vishwakarma, B. D., van Wessem, J. M., Wiese, D., van der Wal, W., and Wouters, B.: Mass balance of the Greenland and Antarctic ice sheets from 1992 to 2020, Earth System Science Data, 15, 1597–1616, https://doi.org/10.5194/essd-15-1597-2023, 2023.

Ray, J., Griffiths, J., Collilieux, X., and Rebischung, P.: Subseasonal GNSS positioning errors, Geophysical Research Letters, 40, 5854–5860, https://doi.org/10.1002/2013GL058160, 2013.

Ray, R. D. and Ponte, R. M.: Barometric tides from ECMWF operational analyses, Annales Geophysicae, 21, 1897–1910,
700   https://doi.org/10.5194/angeo-21-1897-2003, 2003.

Ray, J.and Altamimi, Z., Collilieux, X., and van Dam, T.: Anomalous harmonics in the spectra of GPS position estimates, GPS Solutions, 12, 55–64, https://doi.org/10.1007/s10291-007-0067-7, 2008.

Raymond, C. A., Ivins, E. R., Heflin, M. B., and James, T. S.: Quasi-continuous global positioning system measurements of glacial isostatic deformation in the Northern Transantarctic Mountains, Global and Planetary Change, 42, 295–303,
705   https://doi.org/10.1016/j.gloplacha.2003.11.013, 2004.

Rülke, A., Dietrich, R., Capra, A., Cisak, J., Dongchen, E., Eiken, T., Fox, A., Hothem, L. D., Johnston, G., Malaimani, E., A.J., M., Milinevsky, G., Schenke, H.-W., Shibuya, K., Sjöberg, L. E., Zakrajsek, A., Fritsche, M., Groh, A., Knöfel, C., and Scheinert, M. .: The Antarctic Regional GPS Network Densification: Status and Results, in: IAG 150 Years, edited by Rizos, C. and Willis, P., pp. 133–139, Springer International Publishing, Cham, 2015.

710   Samrat, N. H., King, M. A., Watson, C., Hooper, A., Chen, X., Barletta, V. R., and Bordoni, A.: Reduced ice mass loss and three-dimensional viscoelastic deformation in northern Antarctic Peninsula inferred from GPS, Geophysical Journal International, 222, 1013–1022, https://doi.org/10.1093/gji/ggaa229, 2020.

Samrat, N. H., King, M. A., Watson, C., Hay, A., Barletta, V. R., and Bordoni, A.: Upper Mantle Viscosity Underneath Northern Marguerite Bay, Antarctic Peninsula Constrained by Bedrock Uplift and Ice Mass Variability, Geophysical Research Letters, 48, e2021GL097 065,
715   https://doi.org/10.1029/2021GL097065, e2021GL097065 2021GL097065, 2021.

Savchyn, I., Brusak, I., and Tretyak, K.: Analysis of recent Antarctic plate kinematics based on GNSS data, Geodesy and Geodynamics, 14, 99–110, https://doi.org/10.1016/j.geog.2022.08.004, 2023.

Scheinert, M., Ivins, E., Dietrich, R., and Rülke, A.: Vertical Crustal Deformation in Dronning Maud Land, Antarctica: Observation versus Model Prediction, pp. 357–360, Springer Berlin Heidelberg, Berlin, Heidelberg, https://doi.org/10.1007/3-540-32934-X_44, 2006.

720   Scheinert, M., Engels, O., Schrama, E. J. O., van der Wal, W., and Horwath, M.: Geodetic observations for constraining mantle processes in Antarctica, in: Geochemistry and Geophysics of the Antarctic Mantle, edited by Maritn, A. P. and van der Wal, W., pp. 295–313, Geological Society Memoir, London, https://doi.org/10.1144/m56-2021-22, 2023.

Sušnik, A., Dach, R., Villiger, A., Maier, A., Arnold, D., Schaer, S., and Jäggi, A.: CODE reprocessing product series, https://doi.org/10.7892/boris.80011, 2016.

725   Thomas, I. D., King, M. A., Bentley, M. J., Whitehouse, P. L., Penna, N. T., Williams, S. D. P., Riva, R. E. M., Lavallee, D. A., Clarke, P. J., King, E. C., Hindmarsh, R. C. A., and Koivula, H.: Widespread low rates of Antarctic glacial isostatic adjustment revealed by GPS observations, Geophysical Research Letters, 38, https://doi.org/10.1029/2011GL049277, 2011.

Tregoning, P. and Watson, C.: Atmospheric effects and spurious signals in GPS analyses, Journal of Geophysical Research: Solid Earth, 114, 2009.

Tregoning, P., Twilley, B., Hendy, M., and Zwartz, D.: Monitoring Isostatic Rebound in Antarctica with the Use of Continuous Remote GPS Observations, GPS Solutions, 2, 70–75, https://doi.org/10.1007/PL00012759, 1999.

Tregoning, P., Welsh, A., McQueen, H., and Lambeck, K.: The search for postglacial rebound near the Lambert Glacier, Antarctica, Earth, Planets and Space, 52, 1037–1041, https://doi.org/10.1186/BF03352327, 2000.

VanderPlas, J. T.: Understanding the Lomb–Scargle Periodogram, The Astrophysical Journal Supplement Series, 236, 16, https://doi.org/10.3847/1538-4365/aab766, 2018.

Vardić, K., Clarke, P. J., and Whitehouse, P. L.: A GNSS velocity field for crustal deformation studies: The influence of glacial isostatic adjustment on plate motion models, Geophysical Journal International, 231, 426–458, https://doi.org/10.1093/gji/ggac047, 2022.

Vázquez Becerra, G. E.: Geodesy in Antarctica: A Pilot Study Based on the TAMDEF GPS Network, Victoria Land, Antarctica, Ph.D. thesis, Ohio State University. Division of Geodetic Science, 2009.

Webb, F. H. and Zumberge, J. F.: An introduction to GIPSY/OASIS-II precision software for the analysis of data from the Global Positioning System, Jet Propulsion Laboratory, Pasadena, California, 1995.

Wessel, P., Luis, J. F., Uieda, L., Scharroo, R., Wobbe, F., Smith, W. H. F., and Tian, D.: The Generic Mapping Tools Version 6, Geochemistry, Geophysics, Geosystems, 20, 5556–5564, https://doi.org/10.1029/2019GC008515, 2019.

Whitehouse, P., Clarke, P. J., Koulali, A., King, M. A., Wilson, T. J., Saddler, D. M., Maxfield, D. J., Nylen, T., and Pettit, J.: UKANET: Logistical Challenges and Preliminary Results from a Geodetic Network Recording Crustal Deformation in Antarctica, in: AGU Fall Meeting Abstracts, vol. 2020, pp. C032–11, 2020.

Whitehouse, P. L.: Glacial isostatic adjustment modelling: historical perspectives, recent advances, and future directions, Earth Surface Dynamics, 6, 401–429, https://doi.org/10.5194/esurf-6-401-2018, 2018.

Wilson, T., Bevis, M., et al.: Understanding themismatch between measured and model-predicted crustal motions across West Antarctica: Insights from POLENET-ANET GPS results, in: Workshop on Glacial Isostatic Adjustment, Ice Sheets, and Sea-level Change–Observations, Analysis, and Modelling, pp. 24–26, 2019.

Wolstencroft, M., King, M. A., Whitehouse, P. L., Bentley, M. J., Nield, G. A., King, E. C., McMillan, M., Shepherd, A., Barletta, V., Bordoni, A., Riva, R. E., Didova, O., and Gunter, B. C.: Uplift rates from a new high-density GPS network in Palmer Land indicate significant late Holocene ice loss in the southwestern Weddell Sea, Geophysical Journal International, 203, 737–754, https://doi.org/10.1093/gji/ggv327, 2015.

Zanutta, A., Negusini, M., Vittuari, L., Cianfarra, P., Salvini, F., Mancini, F., Sterzai, P., Dubbini, M., Galeandro, A., and Capra, A.: Monitoring geodynamic activity in the Victoria Land, East Antarctica: Evidence from GNSS measurements, Journal of Geodynamics, 110, 31–42, https://doi.org/10.1016/j.jog.2017.07.008, 2017.

Zanutta, A., Negusini, M., Vittuari, L., Martelli, L., Cianfarra, P., Salvini, F., Mancini, F., Sterzai, P., Dubbini, M., and Capra, A.: New Geodetic and Gravimetric Maps to Infer Geodynamics of Antarctica with Insights on Victoria Land, Remote Sensing, 10, https://doi.org/10.3390/rs10101608, 2018.

Zumberge, J. F., Heflin, M. B., Jefferson, D. C., Watkins, M. M., and Webb, F. H.: Precise point positioning for the efficient and robust analysis of GPS data from large networks, Journal of Geophysical Research: Solid Earth, 102, 5005–5017, https://doi.org/10.1029/96JB03860, 1997.
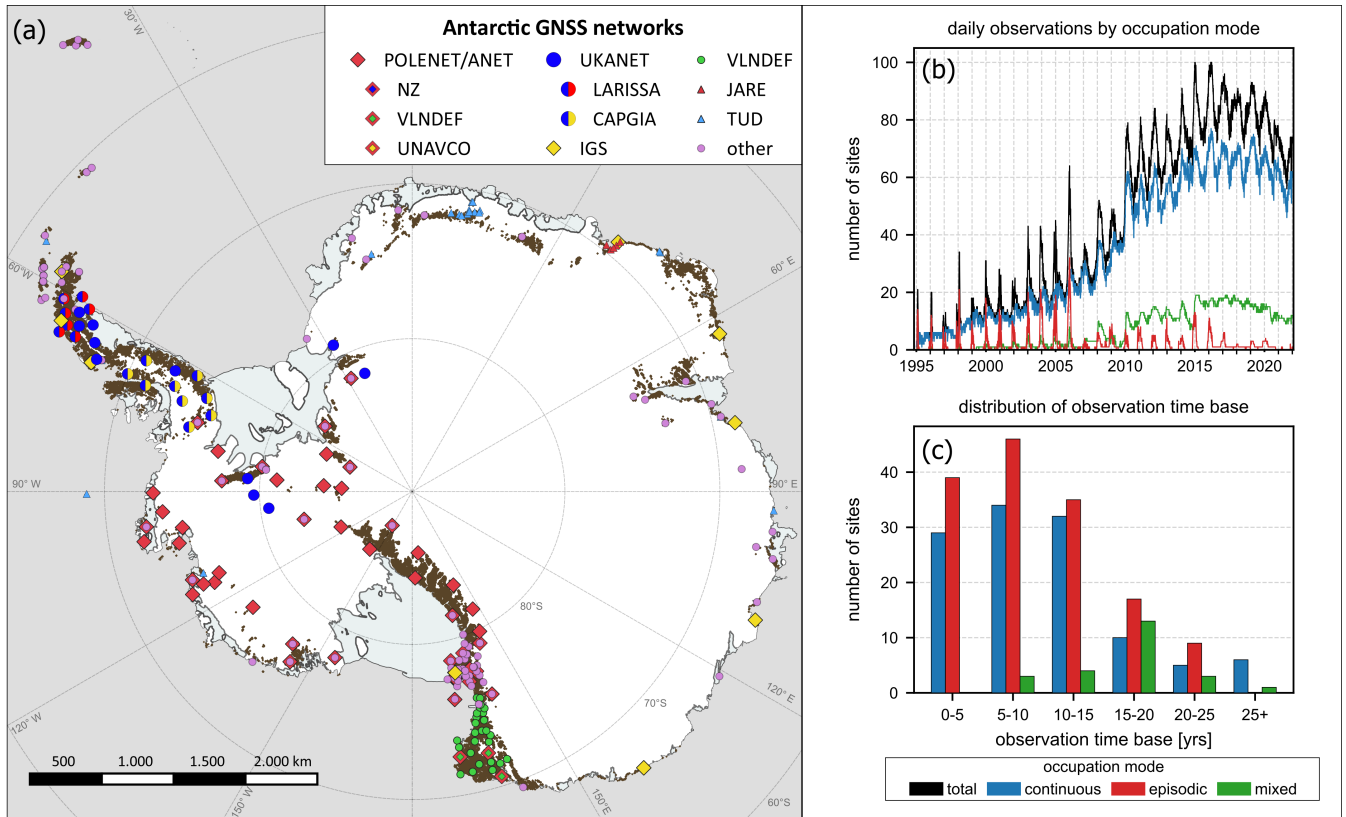
Figure 1. (a) Spatial distribution of GNSS sites on bedrock and selected network affiliations. Bedrock outcrops are indicated in brown (Burton-Johnson et al., 2016). The association of a GNSS site to a network is generally not unique, since sites can be attributed to multiple networks at a time or former networks were integrated in newly established ones. The temporal development of the observation data (b) reveals a steady increase in the amount of data up to 2016. Following the International Polar Year (IPY) in 2008/2009 a strong increase in observations of cGPS sites in particular can be seen, while the number of eGPS observations has decreased significantly. The occupation type "mixed" refers to sites that were initially installed as episodic sites and later upgraded to continuously operating installations. The observation time base (c) results from the difference between the first and last observation and, therefore, does not contain any information about the temporal coverage within the observation period.
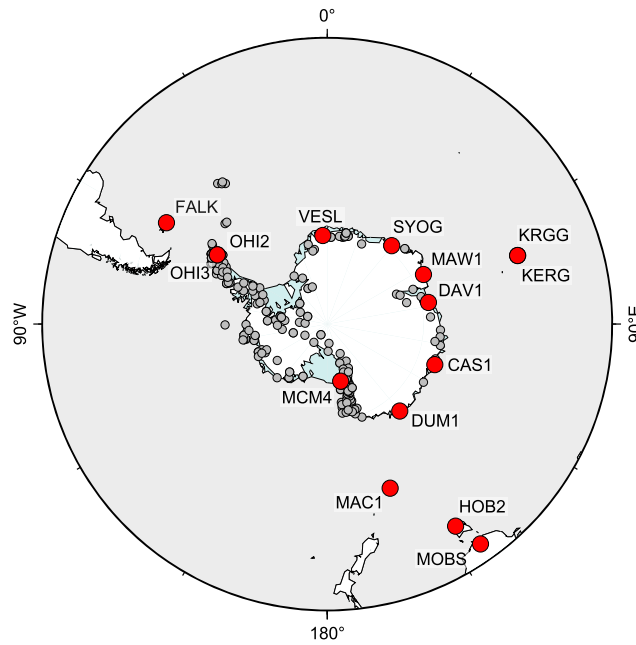
Figure 2. A selection of regionally distributed IGS reference sites to estimate Helmert parameters of individual AC solutions w.r.t. the IGb14 reference frame.
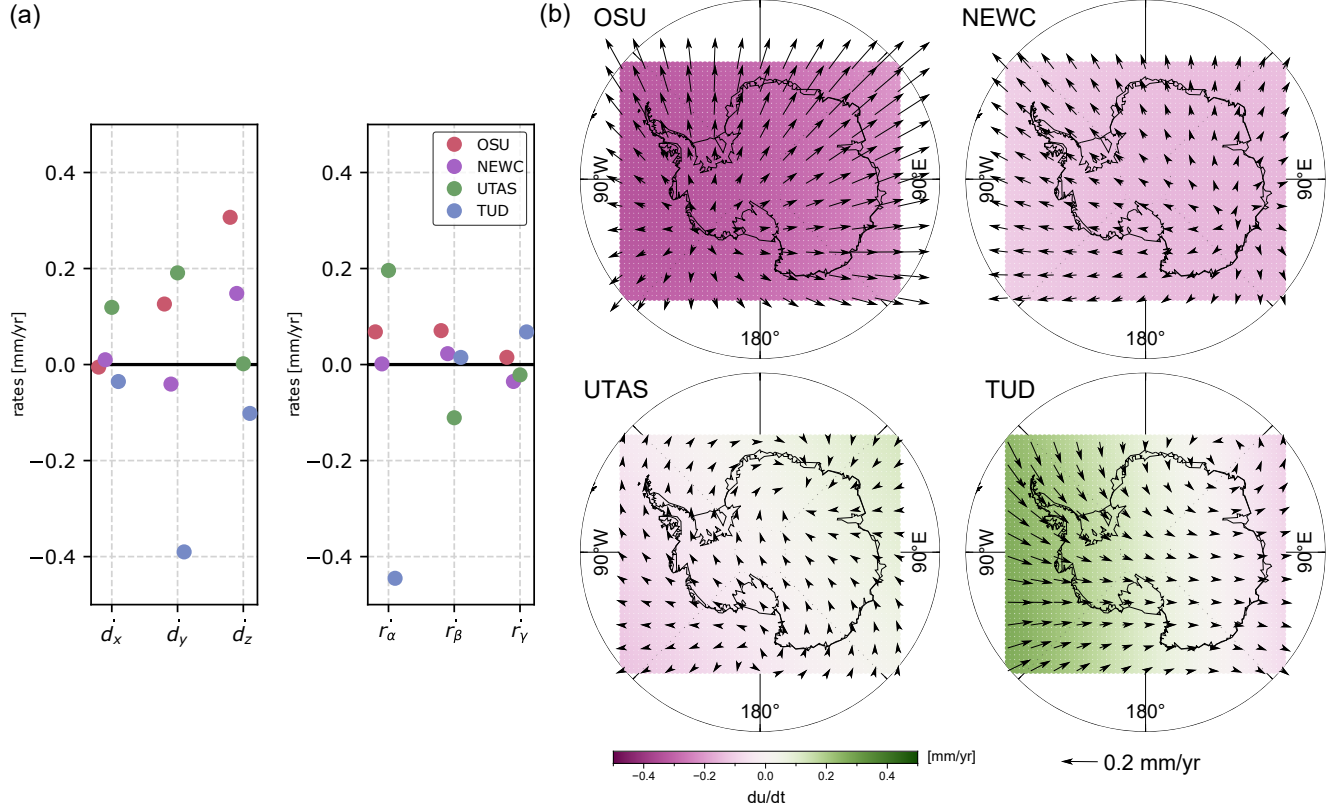
Figure 3. (a) Linear rates of the six Helmert Parameters for AC solutions w. r. t. IGb14 based on a selection of regionally distributed IGS sites. Angular velocities $\dot{\alpha}_j$, $\dot{\beta}_j$, $\dot{\gamma}_j$ are multiplied by the Earth radius to obtain tangential velocities $\dot{r_\alpha}$, $\dot{r_\beta}$ and $\dot{r_\gamma}$ for better comparability to translation parameters. A positive angle describes a clockwise rotation. The formal uncertainties are negligible, with a range of one to two magnitudes smaller than the estimated values. Panel (b) displays the applied linear rates of HPs on a defined grid covering the study area. The coloured grid displays local uplift rates, arrows show lateral velocities.
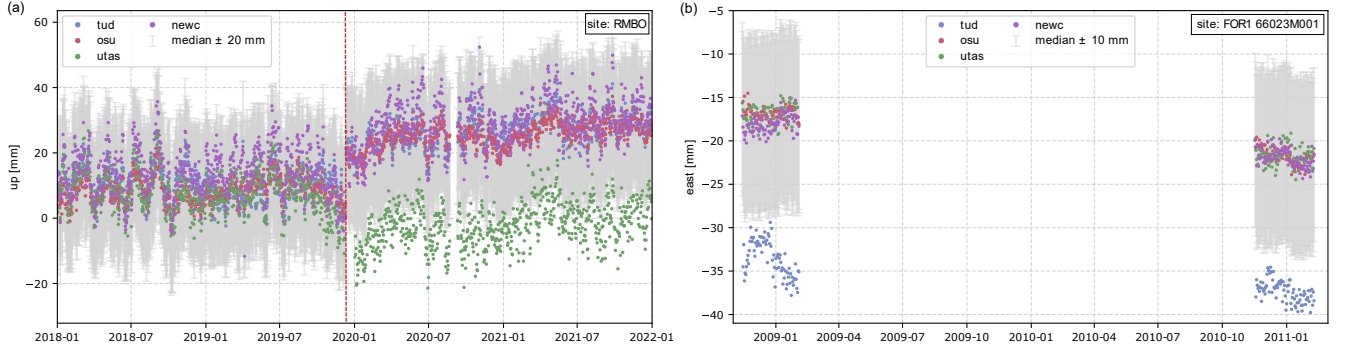
Figure 4. Sections of coordinate time series from the individual AC solutions and the median time series with 20 mm (up) and 10 mm (east) thresholds for the sites (a) RMBO (up component) and (b) FOR1 (east component). Panel (a) shows a systematic bias of the UTAS solution following an equipment upgrade to the Septentrio PolaNt-x-MF antenna and Alertgeo Resolute receiver (11 December 2019). Panel (b) displays the biased east component of the TUD solution, resulting from the correction of the antenna orientation from true north (about 140°), that is only applied in the TUD processing.
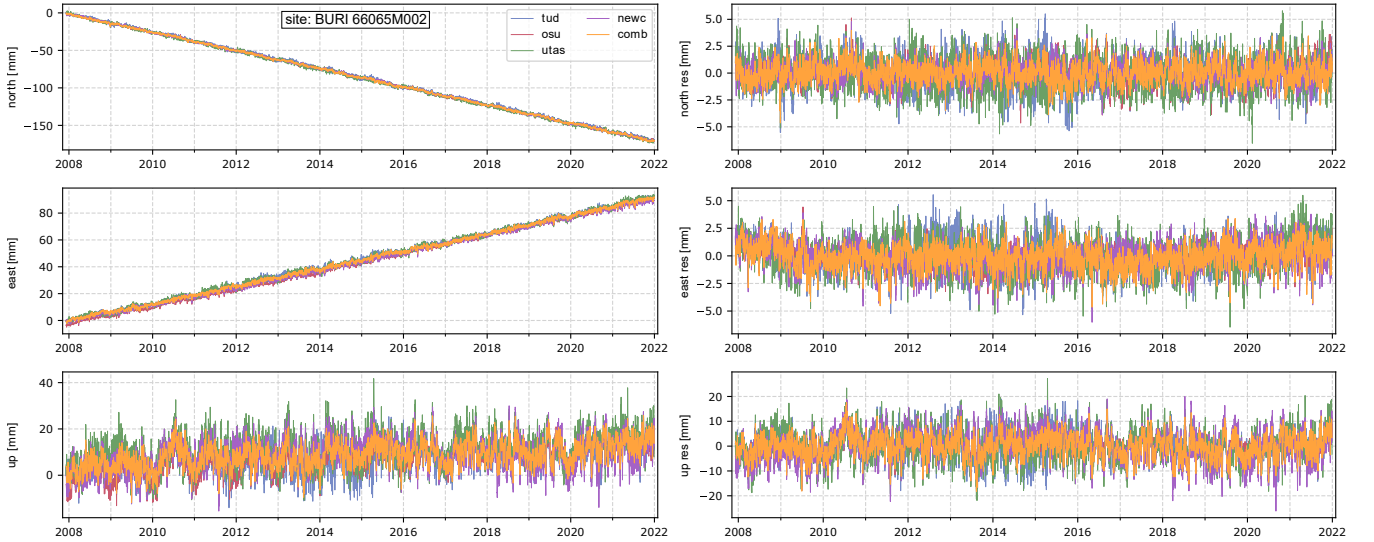
Figure 5. Coordinate time series (a) and the residual time series (b) for the site Butcher Ridge (BURI) from the individual AC solutions and the combined final time series. The RMS of the residual time series of the combined solution yields $1.0\,\text{mm}$, $1.1\,\text{mm}$ and $4.6\,\text{mm}$ for north, east and up, respectively. The individual solutions with lowest RMS reach values of $0.9\,\text{mm}$ (NEWC), $0.9\,\text{mm}$ (OSU) and $3.6\,\text{mm}$ (OSU) for north, east and up respectively.
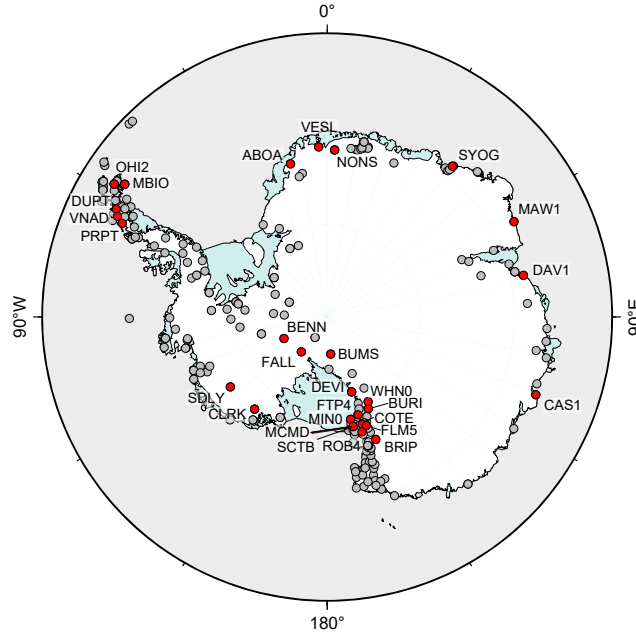
Figure 6. Selection of 29 stable cGPS sites (red) to assess noise characteristics of coordinate time series of the ACs and the combined solution.
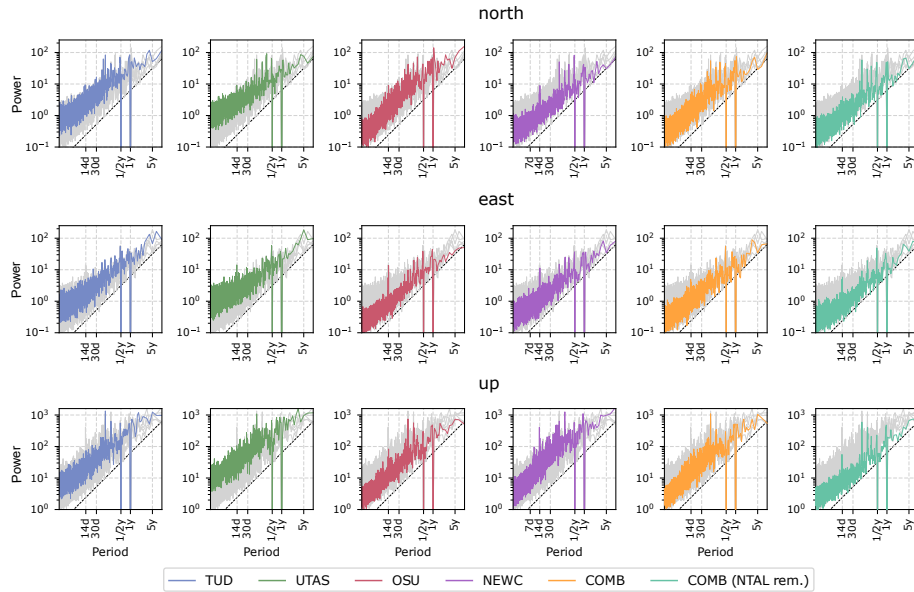
Figure 7. Median Lomb-Scargle periodograms of residual time series (east, north, up) for the selection of 29 cGPS sites for the four ACs and the combined solution with and without NTAL removed. Each plot displays the LSP of a specific solution in color and the LSPs of the other solutions in grey. The dashed line displays flicker noise with an arbitrary amplitude.
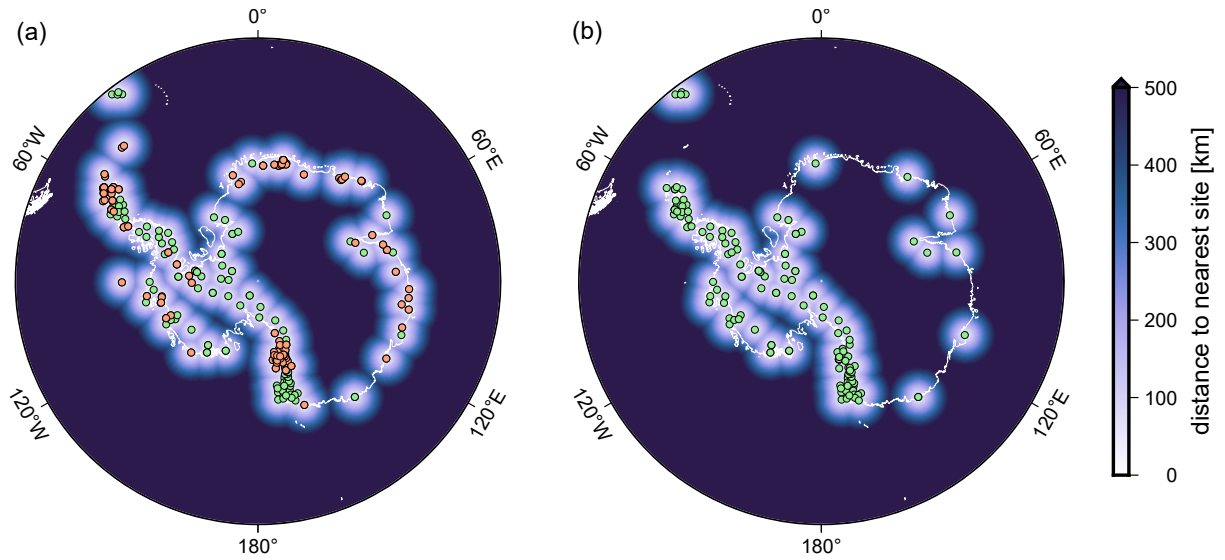
Figure 8. GPS station coverage of (a) the GIANT-REGAIN data set (GR) and (b) the Nevada Geodetic Laboratory (NGL) data set. Green markers indicate GPS sites included in both data sets, while orange sites are only included in the GR data set. The GR data set has an enhanced spatial coverage for East Antarctica from 30°W to 100°E and an increased station density for southern Victoria Land and the northern Antarctic Peninsula.
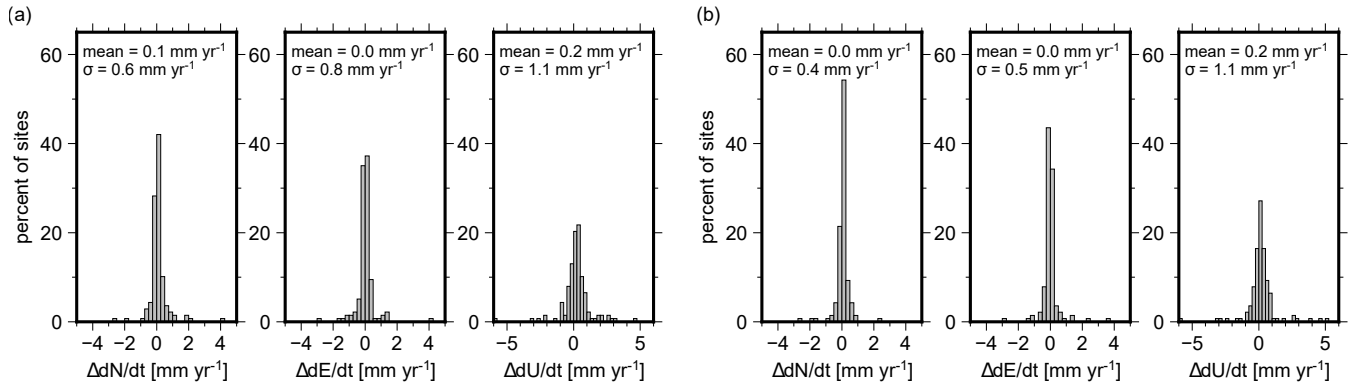
Figure 9. Distribution of differences in estimated linear rates between GR and NGL. In panel (a), the steps in the NGL data set are considered in accordance with the NGL master step file. Conversely, in panel (b), the step information for NGL is consistent with the GR data set.
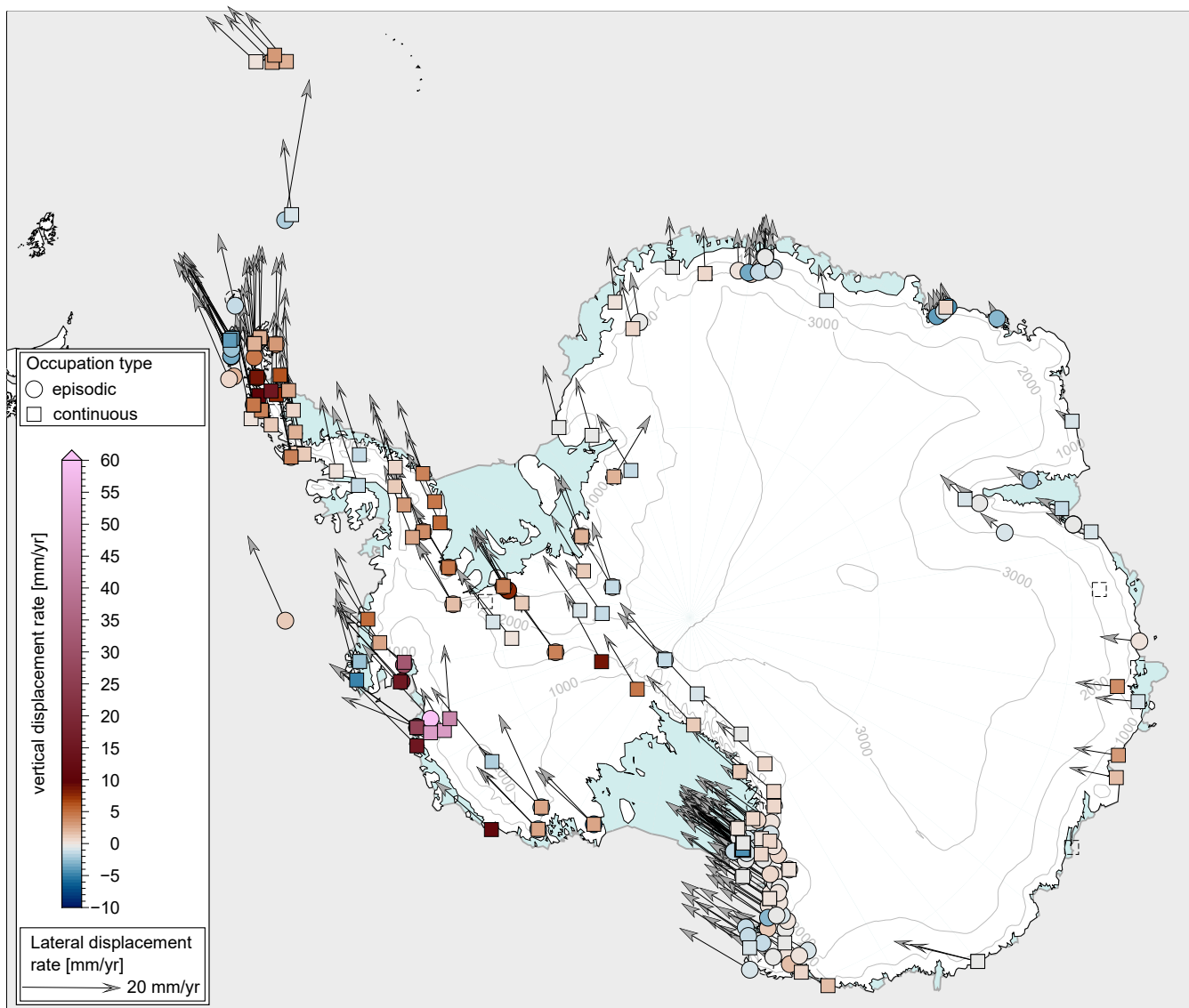
Figure 10. Horizontal and vertical displacement rates resulting from a preliminary analysis of the combined coordinate times series (NTAL removed) using the trajectory model as discussed above. Linear rates were estimated using the Hector software (Bos et al., 2013) using a flicker+white noise model. Only sites with a time base larger 2.5 yr and more than 10 data points were analysed. Note, that these rates still contain all geodynamic effects such as the response of the solid Earth to past and present-day ice-mass loading and unloading, or plate kinematics. Sites are displayed with dashed outlines if no rate was estimated.